ELECTROCHEMICAL IMAGING OF QUANTAL EXOCYTOSIS IN SINGLE CELLS

A Thesis

Presented to

The Faculty of the Graduate School

At the University of Missouri-Columbia

In Partial Fulfillment

Of the Requirements for the Degree

Master of Science

By

SEYEDMEHDI OROUJI

Dr. Kevin Gillis, Thesis Supervisor

December 2015

The undersigned, appointed by the dean of the Graduate School,

have examined the dissertation entitled

ELECTROCHEMICAL IMAGING OF

QUANTAL EXOCYTOSIS IN SINGLE CELLS

Presented by Seyedmehdi Orouji,

A candidate for the degree of

Master of Science

And hereby certify that, in their opinion, it is worthy of acceptance.

Professor Kevin Gillis

Professor Mahmoud Almasri

Professor Li-Qun Gu

ACKNOWLEDGMENT

I owe my gratitude to those who have made this dissertation possible and because of whom my graduate experience has been one that I will cherish forever. Without their help and support I could never been able to finish my dissertation.

First and Foremost, I would like to express my deepest gratitude to my great advisor Dr. Kevin Gillis who is such a decent person and an outstanding scientist. I would like to thank him for his faith in my work, excellent advices, caring, patience, motivations, and providing an excellent atmosphere for all of us in his lab to learn and do research. It is an honor for me to have him as my mentor. His guidance helped me in all the time of research and writing of this thesis. Whenever I faced with an obstacle in my research, he was always available with his great advices to help me to tackle the issue. I could not have imagined having a better advisor and mentor for my study.

I am heartily thankful to Dr. Xin Liu who taught me microfabrication, making device, preparing cells and cell recording. There is no doubt that her help and support was a great blessing for.

I am grateful to know Dr. Almasri and I can't thank him enough for his help, guidance, advices, and providing me with this opportunity to get access to the facilities of his lab.

I have been fortunate to know Dr. Andrew Gu and I would like to sincerely appreciate him for his guidance and help.

In my daily work I have been blessed with a friendly and cheerful group of fellow students and I would like to thank all of them. Especially thanks to Zeke for helping me with making PCBs and cassettes.

I have been amazingly fortunate to know Dr. Naz Islam and Dr. John Gahl who have been very kind to me and supported me during my MS study. If it was not because of them, I would never been able to accomplish my MS. No matter how hard I try, I could never thank them for their kindness and support. Also I would like to thank the electrical and Computer Engineering department for partially supporting me during my MS.

My most sincere appreciation goes to my family and friends who, no matter what, were always there for me. To my lovely sisters and brothers in laws. To my great friends Leila and Soheil who always cheered me up. Above all, I wholeheartedly appreciate my parents for everything they have done for me. Whoever I am or will be, is because of my angel parents.

At last not the least, I want to thank God. The highest and the greatest conscience who miraculously accompanied me through all of the difficulties to be where I am.

Table of Contents

List of Figures

Figure 5- 1. a) The improved design with circular electrodes. b) The previous design with square electrodes…… 84

List of Tables

Abstract

Microelectrodes are widely used in detection of exocytosis events. In order to detect both the time and release location of quantal exocytosis from a single cell, four square microelectrodes located in a 20 μm square microwell were fabricated through photolithographic techniques. A 30 nm thin gold films were used as the material for the microelectrodes and the microwell was fabricated using SU8 thick photoresist. In order to test the quality of microelectrodes, we used cyclic voltammetry technique and the test analyte ferricyanide prior to the amperometry recording. A high density of chromaffin cells were placed in the solution reservoir on top of the electrode arrays, and individual cells were targeted in to the microwells automatically. Poly (L-lysine) was coated on the microelectrode to promote the cells adhesion. Following of that, exocytosis events were triggered by introducing a high potassium concentration to the bath solution. The data obtained from cell recordings were compared with the simulation data obtained from FEM modeling and the locations of release sites were identified. It was observed only sites of quantal releases with relatively high amount of charge (3.59+0.58 pC) can be identified. In order to expand the area on the cell in which the electrochemical imaging is attainable, a simulation-guided electrode re-design was tested using FEM simulations. The results from simulations showed that the improved design, with curved-like electrodes, is predicted to increase the area of detection by approximately 45% compared to the design used in cell tests.

Chapter I. Introduction

1.1. Electrochemistry

Electrochemistry studies the transfer of electrons between a solute in an electrolyte solution and electrodes. The recording acquired from the electrodes can be employed to obtain desired information about an analyte or electrode properties. There are a wide range of electrochemistry applications such as: electrodeposition of metals, battery technology, and measurement of analytes such as blood sugar. One important application of electrochemistry is to study the dynamics of cells. Specifically in this work, we'll study exocytosis of electroactive analytes from single cells rather than population level study due to its capability of single vesicles release detection. Electrochemistry techniques such as amperometry makes it possible to monitor the secretion of single vesicles from single cells and can be utilized to obtain valuable information about the kinetics, location and the amount of the release.

1.2. Exocytosis

Neurotransmitters and hormones are chemicals by which neurons and other cells of the body can communicate with one another. In order to transmit a signal, neurotransmitters are released by the presynaptic neurons and then diffuse through the synaptic cleft to reach to the post synaptic terminals and bind to specific receptors on them. Hormones on the other hand are usually released by endocrine glands and travel through the blood stream to distant tissues and organs so that they can regulate physiological and behavioral activities.

The release of neurotransmitters and hormones is through a mechanism called exocytosis. Exocytosis is an energy-consuming process by which a cell can release the content of its secretory vesicles out to the extracellular space(Breckenridge and Almers 1987). Drugs, toxins and some hereditary disorders can alter the exocytosis events and cause physiological problems (Knight, Tonge et al. 1985, Edwardson, Wang et al. 2003). Unusual exocytosis events can causes neuromuscular junction diseases, neuro-degenerative and psychological disorders. Therefore, understanding

the mechanism of exocytosis is critical to treat these kinds of diseases and also it can make a huge contribution to improve the therapeutic effects of drugs.

During an exocytosis event, the vesicle membrane fuses to the bilayer cell membrane forming a fusion pore and subsequently releases its content(Breckenridge and Almers 1987). This fusion pore formation occurs as a result of large conformational changes in the SNARE (Soluble N-Ethylmaleimide-Sensitive Factor Attachment Protein Receptor) protein complex (Südhof 1995, Butz, Okamoto et al. 1998, Sutton, Fasshauer et al. 1998, Voets, Toonen et al. 2001, Burgoyne and Morgan 2003, Jahn and Scheller 2006). In this process the vSNARE protein (synaptobrevin) on the vesicle interacts with the tSNARE proteins (Syntaxin1 and SNAP25) on the bilayer plasma membrane and form the core SNARE complex which eventually result in fusion pore formation (Figure 1.1). The main hypotheses for exocytosis are full fusion and kiss-and-run (Neher and Marty 1982, De Toledo, Fernandez-Chacon et al. 1993, Albillos, Dernick et al. 1997, Alés, Tabares et al. 1999, Schneider 2001, Klyachko and Jackson 2002). The full fusion hypothesis claims that there is a full and complete fusion between the vesicle and cell membrane following by the full discharge of the vesicle

contents. On the other hand, the kiss-and-run hypothesis suggests that the fusion between the vesicle and cell lipid bilayer is transient and only a portion of the vesicle's content get released and the rest recycles into the cell.

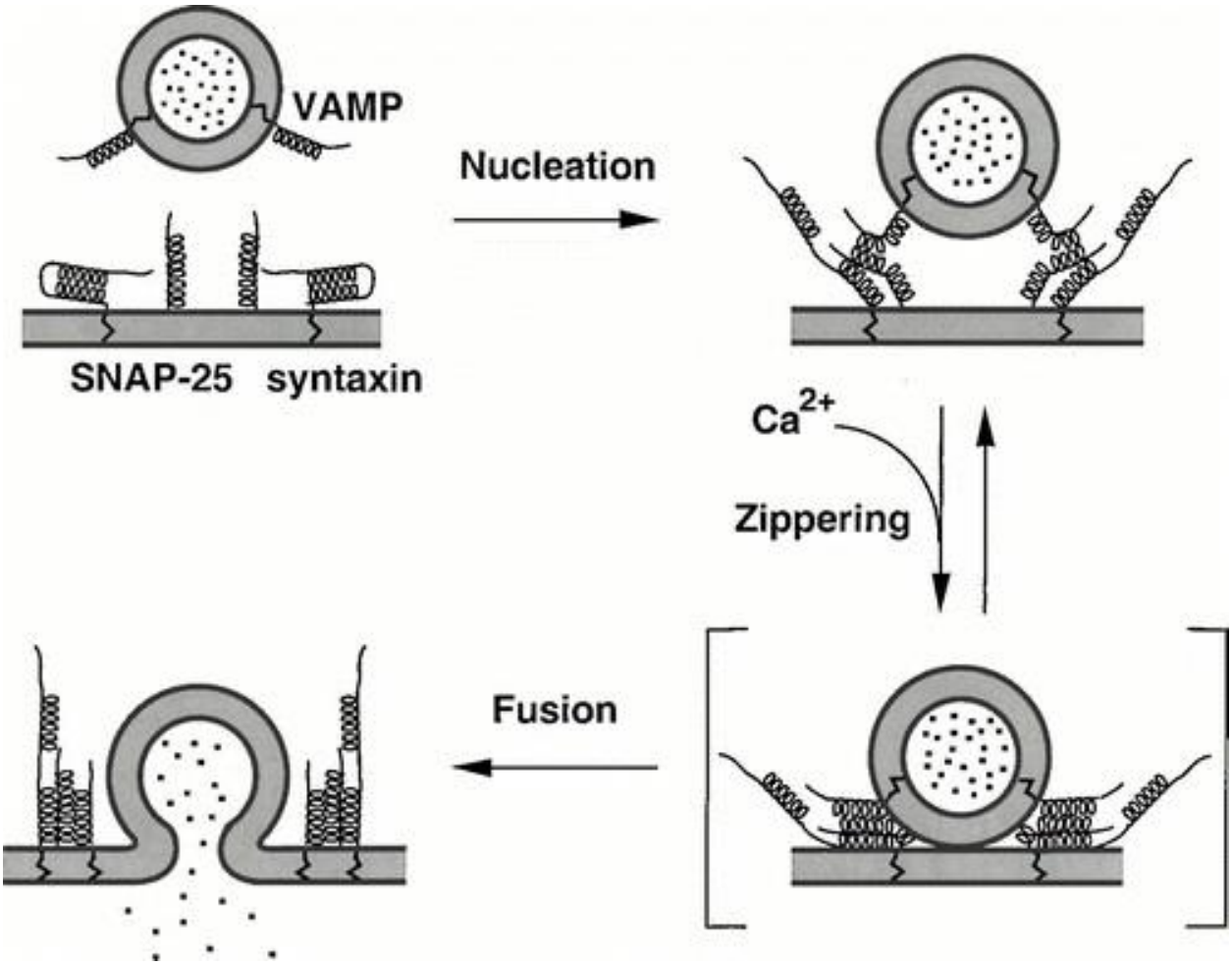

Figure 1- 1. Different stages of exocytosis. 1. Nucleation, 2. Zippering causes the contacts of the vesicle and plasma membranes, 3. Fusion formation(Lin and Scheller 2000).

Bovine chromaffin cells from adrenal glands have been widely used for the study of exocytosis (Gillis, Pun et al. 1991, Wightman, Jankowski et al. 1991, Gillis and Chow 1997). Unlike neuronal cells, the transmitter released from chromaffin cells are

accessible to the electrodes for the redox reaction while their functionality is similar to the neuronal cells. These properties suggest chromaffin cells as a great candidate for the study of neurotransmitter release. Chromaffin cells release catecholamines, which are readily oxidized once they reach to the surface of a working electrode. Catecholamines are secreted by the adrenal glands as part of the “fight or flight” response(Fenwick, Fajdiga et al. 1978) that occurs as a result of a threatening situation.

There are two different types of exocytosis: 1) constitutive exocytosis and 2) Ca+2 triggered, or regulated exocytosis. Constitutive exocytosis occurs in all cells to make the extracellular matrix or to transport newly synthesizing proteins to the plasma membrane. Regulated exocytosis however, occurs due to an external stimulus and an increase in intracellular concentration of [Ca+2]. In excitable cells, membrane depolarization leads to opening of voltage-gated Ca2+ channels and Ca2+ entry into the cell to trigger exocytosis. In chromaffin cells, membrane depolarization results from release of the transmitter acetylcholine from the splanchnic nerve onto the

cells, which opens nicotinic acetylcholine receptor ion channels. Depolarization can be artificially induced by increasing the extracellular concentration of [K+]e.

1.3. Detection of exocytosis

The release of transmitter from single vesicles (quantal exocytosis) can be electrochemically detected using ampertometry techniques (Chow, von Rüden et al. 1992). In this technique a constant voltage between the working electrode (anode) and the reference electrode (cathode) is applied (typically 700 mV) and the current as a function of time is recorded. Catecholamine molecules that contact the surface of a microelectrode are oxidized, resulting in the transfer of two electrons to the electrode. The oxidation of the transmitter (typically a catecholamine or histamine) results in an aperometric spike which sometimes preceded by a "foot signal"(Chow, von Ruden et al. 1992) (Figure 1.2). The foot signal is thought to originate from the slow flux of transmitter through a small fusion pore that later expands to allow rapid release during the spike portion of the signal (Fig. 1-2) (Albillos, Dernick et al. 1997). Thus the amperometry signal gives information about the time course of the fusion event. Amperometry also makes

it possible to quantize the number of catecholamine molecules released during a quantal fusion event(Chow, von Rüden et al. 1992).

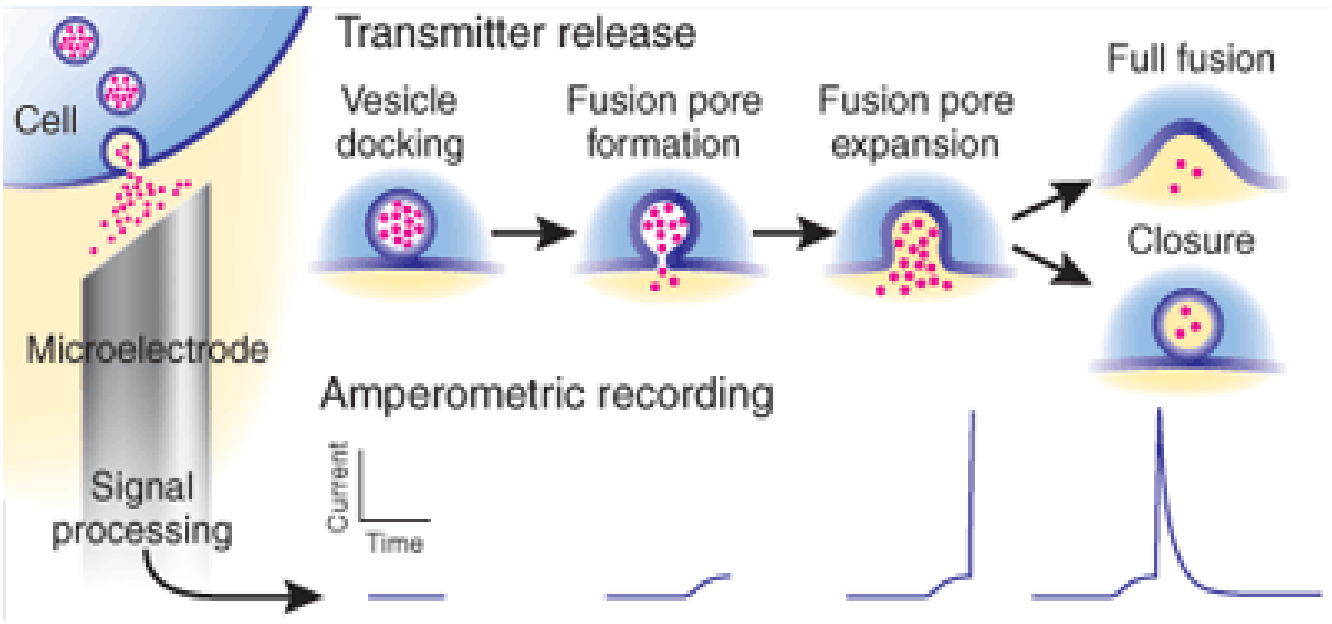

Figure 1- 2. Detection of exocytosis event by using micro electrode. As illustrated can show itself as a foot signal, the expansion can be detected as the big spike and finally after full fusion, the decay part of the spike corresponds to the pore closure(Evanko 2005).

Spike kinetic information is usually quantified by t1/2, trise and tfall. The spike duration at half maximal duration (t1/2) is a good measure of the duration of the release process(Trouillon, Lin et al. 2013). The rise time (trise) is defined as the time difference between 25% and 75% of the signal peak value during the rising part, whereas the fall time (tfall) is the difference between 25% and 75% of the signal peak value on the falling phase of the signal. The rise time is thought to reflect fusion pore opening while the fall time reflects either the exhaustion of vesicle contents or the

closure of the fusion pore. Figure 1-3(a) depicts t1/2, trise and tfall. A typical foot signal is depicted in figure 1-3(b) which for the first time was reported by Chow et al (Chow, von Ruden et al. 1992). Typically a foot signal provides information about the size of a fusion pore and the slow release of vesicular content through a 2-3 nm pore before the expansion of the pore and the rapid release start(Lindau and Alvarez de Toledo 2003).

Carbon fiber electrodes (CFE) are extensively used as the working electrode to detect quantal exocytosis events due to their excellent electrochemical properties. However, in order to obtain high-throughput devices, electrochemical electrode arrays fabricated using MEMS technology have been developed(Smith, Proks et al. 1999).

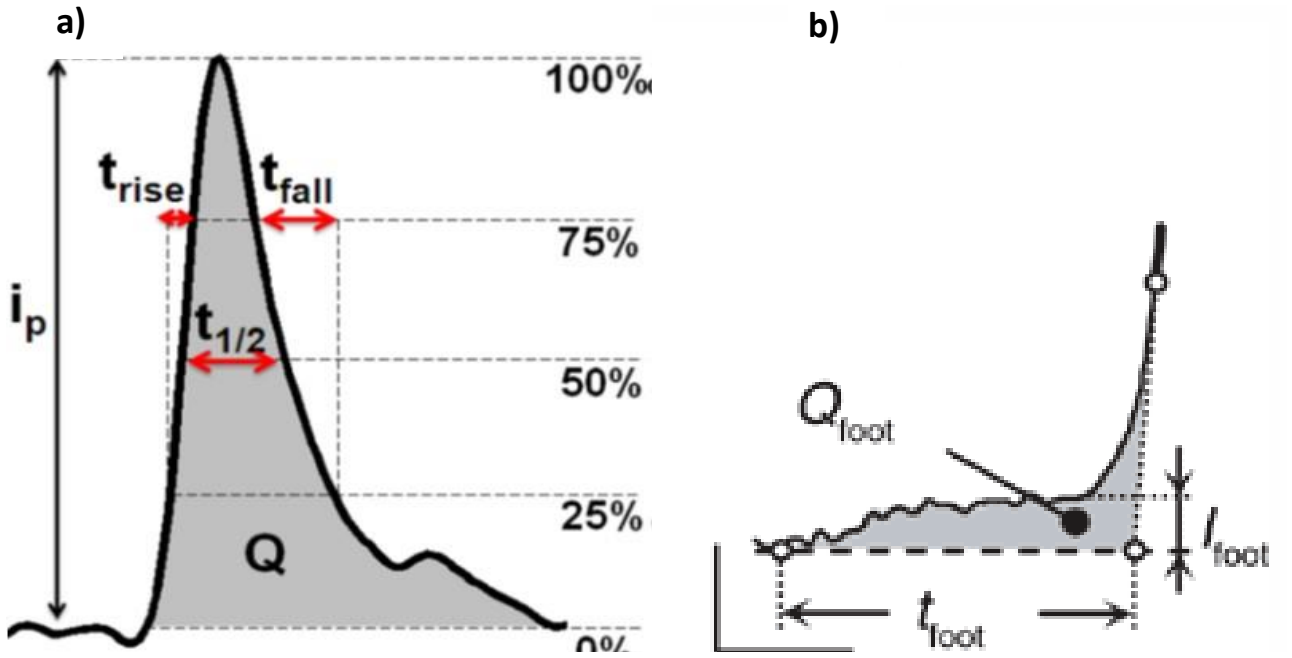

Figure 1- 3. a) t_{rise} is the time difference of 75% and 25% of the peak value in the rising part of the signal. $T_{1/2}$ is the time difference of 50% of the peak value of the rising part and 50% of the peak value of the falling part of the signal. From integrating the area underneath the signal (area shaded with grey) the total electrical charge or released molecules can be obtained. b) The foot signal which can be assigned to the fusion pore formation. (a) G. Ewing 2013, b)Mosharov and Suluzer, 2005)

In addition, in order to allow imaging of the cell release site simultaneously with electrochemical measurement of exocytosis, transparent electrode materials such as Indium Tin Oxide (ITO) and Diamond-Like Carbon (DLC) have been used (Heiskanen, Spégel et al. 2008, Gao, Bhattacharya et al. 2009). Finally, MEMS technology has been used to fabricate electrode arrays around a single cell(Hafez, Kisler et al. 2005). The relative amplitude and time course of spikes originating from the same exocytosis event is compared between the electrodes in order to calculate the location on the cell surface where the vesicle fusion event originated.

1.4. MEMS/BioMEMS

Micro-electro-mechanical Systems (MEMS), also known as Microsystem and Micro-machines, is a field of study of how to make micro scale devices (usually between 1 to 100 micrometers). Since the dimensions of these devices are very small and it is possible to make hundreds of a specific device at the same time with through a batch fabrication process, the unit cost of these devices can be decreased significantly. Moreover, MEMS devices consume small power and/or require small amounts of reagents and have excellent sensitivity. It is due to these benefits that it is estimated that the market of MEMS industry will grow to a $22 billion by 2018(R. Colin Johnson). Examples of MEMS devices include: accelerometers, micro-mirrors, gyroscopes, solar cells, light sensors, drug delivery devices, biosensors, and cell sensors (Ho and Tai 1996, Santini, Richards et al. 2000, Abel and von Woedtke 2002, Grayson, Shawgo et al. 2004, Nguyen and Wu 2005, Tanaka 2007, Bogue 2013).

Biological Micro-Electro Mechanical Systems (BioMEMS) is an emerging technology field. Due to the low price per unit of these devices they can be disposed after each use which significantly reduces the chance of infection in medical devices. Owing to

the small size of BioMEMS devices and the small consumption of the reagent, they have become a great candidate for implantable medical devices and biosensors.

Microelectrode arrays have been widely used in BioMEMS research programs as well as in commercial devices. Due to their cost efficiency, fast response and high sensitivity, microelectrodes have become a great candidate for detecting and measuring very small currents. In particular, the noise variance of a microelectrode scales with area(Yao and Gillis 2012), therefore micrometer-scale electrodes can resolve pA-scale currents with adequate signal-to-noise ratio.

1.5. Objective

In order to detect both the time and release location of quantal exocytosis from a single cell, a technique where four electrodes surround a single cell has been developed (Hafez, Kisler et al. 2005). Figure 1-4 depicted the fabricated device without the cell.

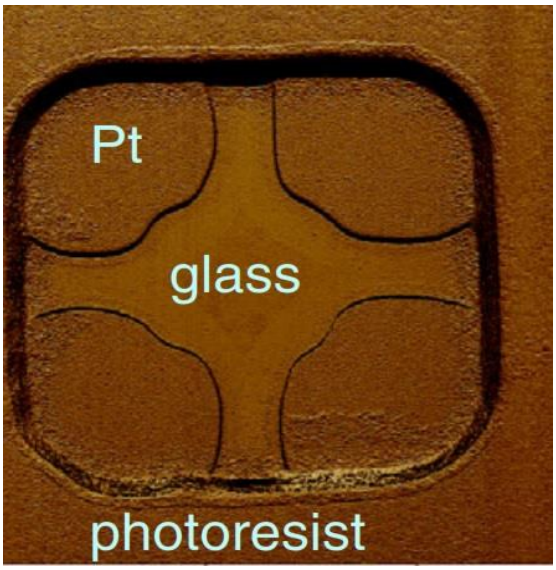

Figure 1- 4. Fabricated device with four electrodes.(Dias, Dernick et al. 2002)

In this method we need to make two important assumptions: 1. the diffusion of the released catecholamine molecules is isotropic and 2. All four electrodes are equally effective at oxidizing all the molecules arriving on their surfaces(Hafez, Kisler et al. 2005). To localize a quantal release event, we need to obtain a measurable spike

signal from at least three electrodes. The relative size and time course of the signal from each electrode is then used to determine the release site. In other words, if release occurs closest to electrode 1, this electrode will have the largest spike whereas the electrode furthest from the release site will record a very small spike.

Quantification of the release site is carried out as follows. First, a random walk simulation (RWS) is performed to predict the signal recorded in each of the four electrodes for an impulse release event located at a specific location on the chip. The release location is then systematically moved throughout a grid pattern over the surface of the chip and a family of predicted recordings is compiled from the RWS. Since each fabricated chip varies slightly, the simulations are repeated for the geometry of each electrode array. In the next step, each actual release event recorded from the set of electrodes is compared to the RWS, and the grid location that gives the least-squares fit of the RWS to the event data is chosen as the release site. A limitation of this method is that it can only localize exocytosis events that originate very near the center of the electrode array (Hafez, Kisler et al. 2005) because it is necessary to obtain a measurable signal in at least three electrodes in order to

“triangulate” the position. Another limitation is that chromaffin cells need to be individually manipulated to the appropriate location in the center of the electrode array using a pipette and a micromanipulator. This approach, however, is time consuming and doesn’t ensure tight attachment of the cell to the chip, something that is necessary to allow high-resolution imaging and exchange of the solution bathing the cell.

The goal of this thesis is to improve the electrode-array approach in several ways. 1. Automatically targeting the cell to the appropriate location between the four electrodes using a microwell trap, 2. Replace RWS with finite-element solutions of the diffusion equation using COMSOL software in order to greatly decrease the time to execute the simulations and improve their resolution, and 3. Discuss the possibility of the methods that can be employed to expand the area in which the release of the vesicle can be localized using simulation-based design improvements. A final improvement is that we developed a new method for interfacing the glass microchips to the multi-channel amplifier using a “flip chip” bonding of the microchip to a PCB board.

Chapter II. Time dependent diffusion simulation through Finite Element Analysis

2-1. Introduction

The change in concentration with respect to distance is called the concentration gradient. Equation 2-1 shows the mathematical definition of concentration gradient in a one dimentional enviroment.

$$\dot{C} = \frac{\Delta C}{\Delta x} \qquad Eq.\ 2\text{-}1$$

Diffusion is defined as the net movement of a substance as a result of the concentration gradient. In fact, the movement of particles is due to their kinetic energy and is equally possible in all directions. The net displacement of particles however, is due to the concentration gradient. The time that is necessary for these particles to travel to a specific location is called “diffusion delay”.

For high sensitivity it is desirable for the detecting electrode to be close to the release site on the surface of the cell because this results in shorter diffusional delay and larger amplitude electrode response, and thus greater signal-to-noise ratio, following a release event.

In order to localize release events with multiple electrodes, however, it is essential that some of the particles from a release event reach at least several electrodes, therefore no individual electrode can be too close to the release site or else it will oxidize all the analyte. This chapter describes diffusion simulations that allow one to explore the tradeoff between highly sensitive detection and accurate spatial localization of exocytosis with electrode arrays.

Localizing the site of release with electrode arrays through diffusion simulations is an inverse problem. First, we simulate the diffusion of catecholamines and the corresponding currents in each electrode in the array assuming impulse release from a specific point in a grid. Then the simulations are repeated upon relocating the site of release to each point in the grid. Then, we will compare the actual recording from the cell with the simulation results. In other words, we will calculate the mean squared error in the time course of a release event between the experimental data and the data obtained from simulation. Finally we choose the least mean squared error and assign the corresponding point of the grid as the location of the release event.

COMCOL multi-physics is a graphical user interface (GUI) that utilizes finite element methods (FEM) in order to solve PDEs. In this work, COMSOL is used in order to perform the time dependent diffusion simulation of the catecholamine molecules. In order to validate the data obtained from COMSOL, a random walk simulation (RWS)

is coded and the obtained result is compare with the results from COMSOL simulation.

Beside the fact that COMSOL simulation is enormously faster than RWS, it also makes it much easier to make changes in the simulation problem.

2-2. Diffusion

Diffusion is a process in which a substance (atom/molecule/ion) passively spreads out in the surrounding environment as a result of thermal motion. Net movement of the substance occurs due to the concentration gradient where the net flux is in the direction of the lower concentration. The reason lies behind the random nature of the particles' thermal movement. In fact all particles are moving in the all directions at the same time however, due to the fact that the place with higher concentration contains more particles, the probability of having more immigrating particles from that point is higher. Hence, the net flux of the movement is always down to the concentration gradient. The diffusion continues until the system reach to the equilibrium and the concentration gradient becomes zero.

From the phenomenological point of view, the diffusion phenomenon can be describe with the Fick's law of diffusion. By solving the time dependent PDEs, obtained from the Fick's second law, it is possible to describe the diffusion of a substance respect to the time.

Diffusion can also be described at the atomic and molecular level by Random Walk diffusion theory. The random movement of particles, also known as Brownian motion, is not really random since the movement is as a result of the collision between the particles. The overall net movement however, can be described by the random walk theory.

2-2-1. Fick's First Law

Fick's first law states that the relationship between the net flux density of a substance is proportional to the diffusion coefficient and the concentration gradient (Eq. 2-1).

$$J = -D\frac{\partial c}{\partial x} \qquad \textit{Eq.}\ 2\text{-}2$$

Where J $(\frac{mol}{m^2 s})$ is the flux density, D $(\frac{m^2}{s})$ is the diffusion coefficient (which is proportional to the temperature and inversely proportional to the viscosity of the medium and the size of the molecule), $C(\frac{mol}{m^3})$ is the concentration of the substance and $x(m)$ is the position. The negative sign of this formula means that the diffusion direction is in the direction that the concentration decreases.

Equation 2-2 is for one-dimensional diffusion. In order to generalize it for all dimensions, it can be written as:

$$J = -D\nabla C$$

Eq. 2-3

In this case the *J* is the diffusional flux vector.

2-2-2. Fick's Second Law

Fick's first law describes the diffusion under the assumption of steady state. Fick's second law on the other hand, describes the diffusion as a function of time and position.

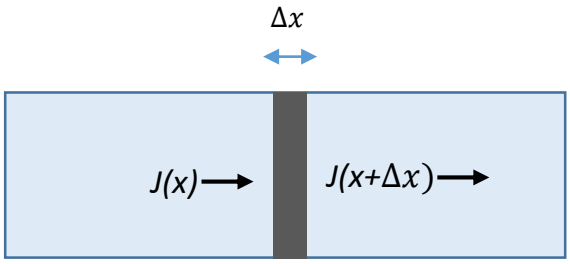

Figure 2- 1

Due to the mass conservation law, the change of the concentration over the time Δt can be written as:

$$\frac{\Delta C}{\Delta t} = \frac{J(x) - J(x + \Delta x)}{\Delta x} \qquad \textit{Eq}.\ 2\text{-}4$$

For $\Delta t, \Delta x$ going to zero the equation can be restate as:

$$\frac{\partial C}{\partial t} = -\frac{\partial J(x)}{\partial x} \qquad \textit{Eq}.\ 2\text{-}5$$

Hence, by substituting J from equation 2-2, Fick's second law would be:

$$\frac{\partial C}{\partial t} = D\frac{\partial^2 C(x)}{\partial x^2} \qquad \textit{Eq}.\ 2\text{-}6$$

Equation 2-6 is a PDE that determines the concentration in both time and location. Again, this equation is for one-dimensional diffusion. The more general form of Fick's second law is expressed as:

$$\frac{\partial C}{\partial t} = D\nabla^2 C \qquad \textit{Eq.}\ 2\text{-}7$$

In order to solve the PDE of Fick's second law, we need two boundary conditions and an initial condition. As an example, for a one-dimensional case and boundary conditions of:

1. $C(x,0) = C_0$
2. $C(0,t) = C_s$
3. $C(\infty,t) = C_0$

The solution of the differential equation is:

$$\frac{C(x,t) - C_s}{C_0 - C_s} = \mathrm{erf}\left(\frac{x}{2\sqrt{Dt}}\right) \qquad \textit{Eq.}\ 2\text{-}8$$

Where $\mathrm{erf}(z)$ is:

$$\mathrm{erf}(z) = \frac{2}{\pi}\int_0^z e^u du \qquad \textit{Eq.}\ 2\text{-}9$$

Since analytically solving the PDEs is fairly complicated (and in many cases impossible) for complex geometries, Finite Element Analysis can be employed in order to obtain a good approximation of the solution.

2-3. Finite Element Method (FEM)

The invention of the Finite element method (FEM) returns back to the 1950s in order to solve complex elasticity problems for complex geometries. FEM is a technique that tries to numerically solve an approximation of PDEs. In this method, the volume of interest is divided into in to many small elements through a process called mesh generation. The elements are sufficiently small so that the quantity of interest, in this case concentration, is approximately constant across the element, and the differential equation is approximated by a difference equation. Since a finer mesh allows a better approximation of a differential equation the final approximate solution will be more accurate. A smaller meshing size, however, is computationally more expensive because the fundamental difference equations are applied to every element. Therefore, there is a tradeoff between precision and the speed of performing the simulation. After representing all these elements with the governing equations and boundary conditions, a set of global finite element equations are formed. These finite element equations are applied iteratively until the solution converges.

2-4. COMSOL simulation for the Electrochemical Imaging technique

“Electrochemical imaging” refers to an approach for determining the location of single-vesicle release events by comparing the magnitudes and time courses of the amperometric current measured by multiple electrodes surrounding a cell. Each working electrode oxidizes a portion of the molecules released by a fusion event with the electrode located closest to the release event capturing the most molecules with the shortest diffusional delay. The electrodes and the well of the fabricated device are depicted in the figure 2-2.

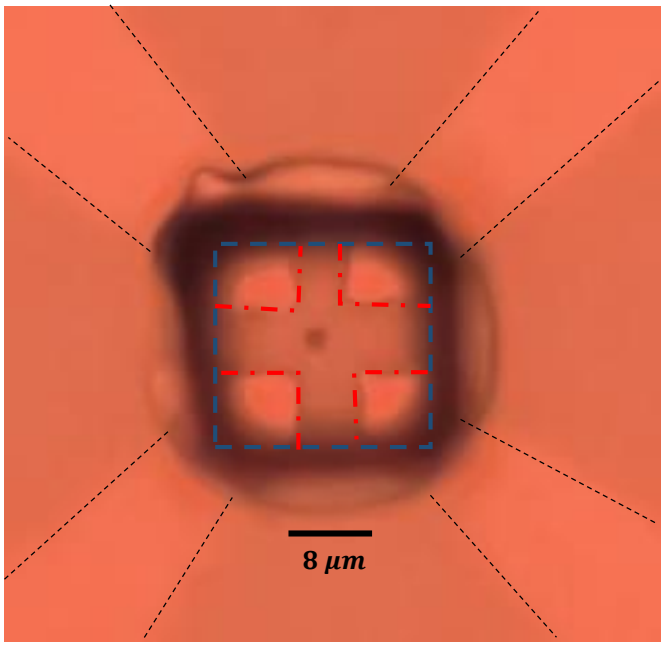

Figure 2- 2. Photomicrograph of an electrode array surrounding a microwell cell “trap”. 1) The metal films are shown with black dashes. 2) Working electrodes are squares with the length of 8 um shown with red dashes. 3) The blue dashed square depicts the well opening in the SU-8 insulating film.

The first step in order to perform the diffusion simulation in COMSOL is to define the dimension of the simulation volume as well as the physics of the problem. The Transport of Diluted Species (tds) physics of COMSOL includes the governing

equations of diffusion, therefore it is used as the physics interface of the problem. This interface is used to compute the concentration field of a dilute solute in a solvent. Since the kinetic information of the problem is essential for spaitio-temporal detection of the event, time-dependent simulations are performed.

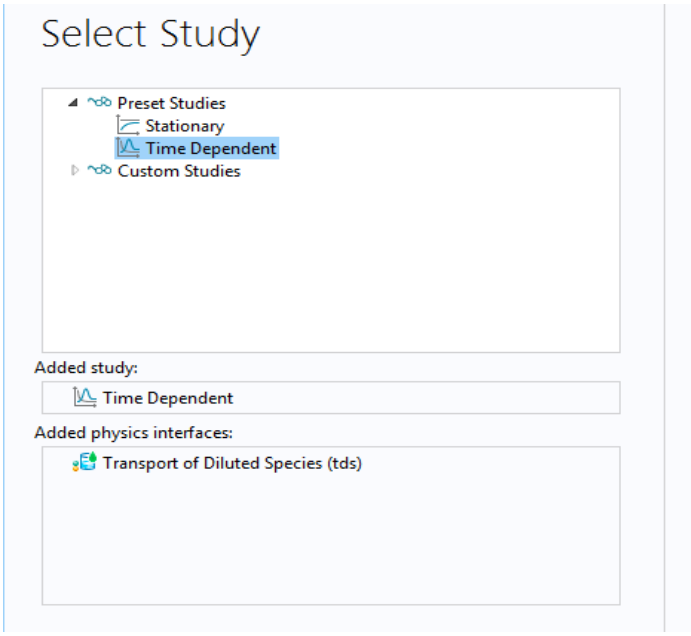

Figure 2- 3. Choosing the Physics interface and study type in COMSOL

2-4-1. Geometry

In order to obtain reliable results from simulation, it is substantially important to make the geometry of the simulated device as similar as possible to the fabricated device. Therefore, measurements from a photo of the actual (Figure2-2) device were used for the model.

As depicted in figure 2-4, a solid box with the size of 20x20x15μm(LxWxH) was made in order to model the geometry of the SU8 well in which the simulation is performed.

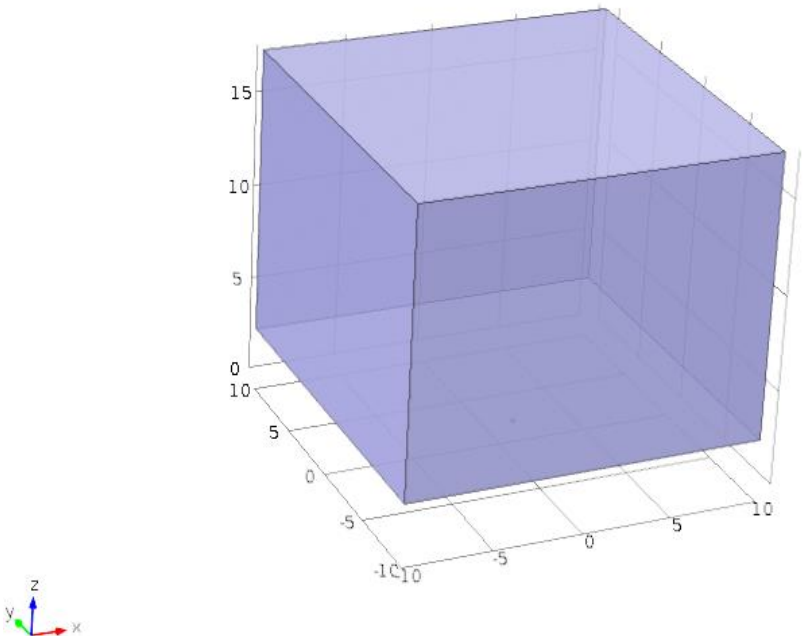

Figure 2- 4. SU8 well is modeled with a solid box with the dimension of 20x20x15μm(LxWxH)

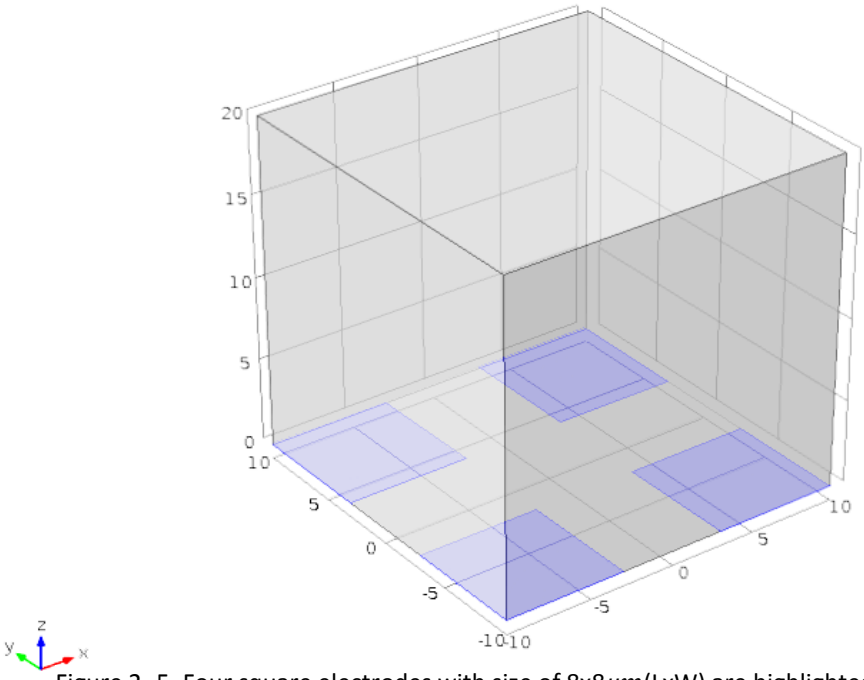

Figure 2- 5. Four square electrodes with size of 8x8μm(LxW) are highlighted

Then the electrodes with the size of 8x8 μm square were added to the main geometry (Figure 2-5 shows the highlighted electrodes).

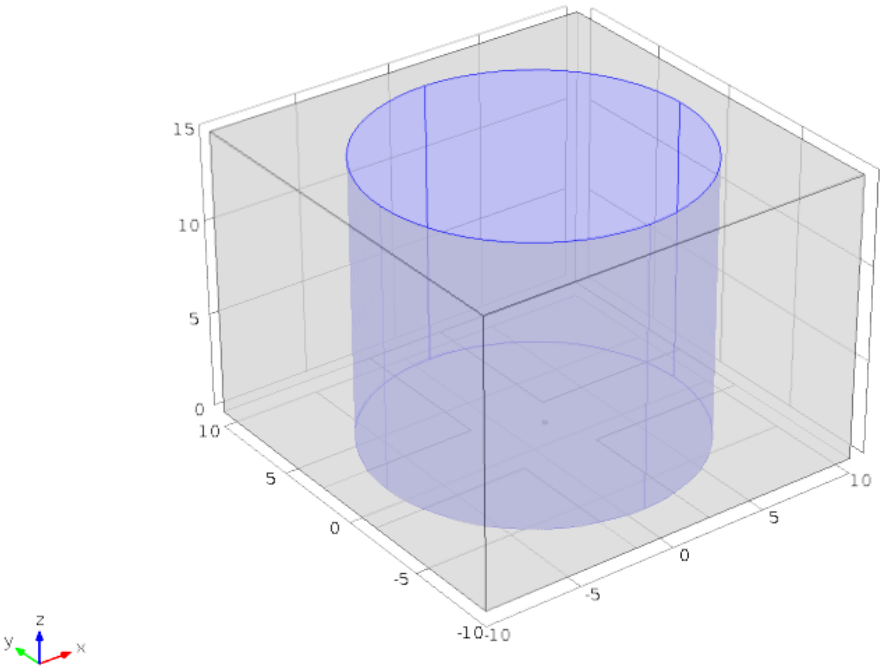

Figure 2- 6. The Chromaffin cell, modeled with a semi-infinite cylinder with radius of 8 μm

In order to model the Chromaffin cell, a semi-infinite cylinder (Figure 2-6. Highlighted by blue) with the radius of 8 μm (similar to the Chromaffin cells) was created suspending 0.4 μm above the floor of SU8 box.

Finally the area of the release was modeled by a sphere with a radius of 120 nm(Glavinović, Vitale et al. 1998) (similar to the size of a chromaffin granule) at the bottom of the cell. The final result of the geometry is depicted in figure 2-7.

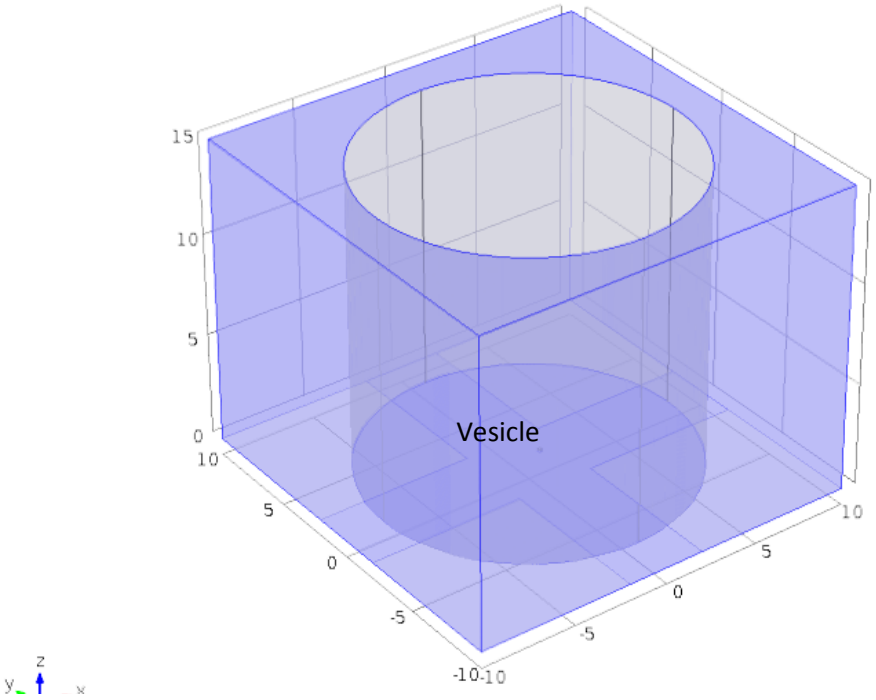

Figure 2- 7. The modeled geometry of the fabricated device. The vesicles is shown by red dot at the (X=1, Y=0.5, Z=0.4) μm

2-5-1. Initial and Boundary Conditions

The governing equations in transport of diluted spices module for time dependent problem is Fick's second law (eq. 2-8)

$$\frac{\partial c}{\partial t} + \nabla.(-D\nabla c) = R \qquad \textit{Eq.}\ 2\text{-}10$$

Where *R* ($\frac{mol}{m^3 \cdot s}$) is a reaction rate expression for the species.

Here c is the concentration of unoxidized catecholamine. Eq.2-10 allows the diffusion coefficient (D) to vary by position, although a constant value was used in the simulations. A value of $8 \times 10^{-7}\ \frac{cm^2}{s}$ was chosen based on measurements of catecholamine diffusion in the extracellular space (Hafez, Kisler et al. 2005).

In order to solve the time-dependent diffusion equation, we need to define the initial and boundary conditions for each feature in the model geometry. The initial concentration of the diluted species (catecholamines) throughout the model geometry was set to zero except the small sphere that represents the release site.

$$c(x, y, z) = 0\ at\ t = 0, x, y, z \neq vesicle(x, y, z) \quad \text{(Initial condition 1)}$$

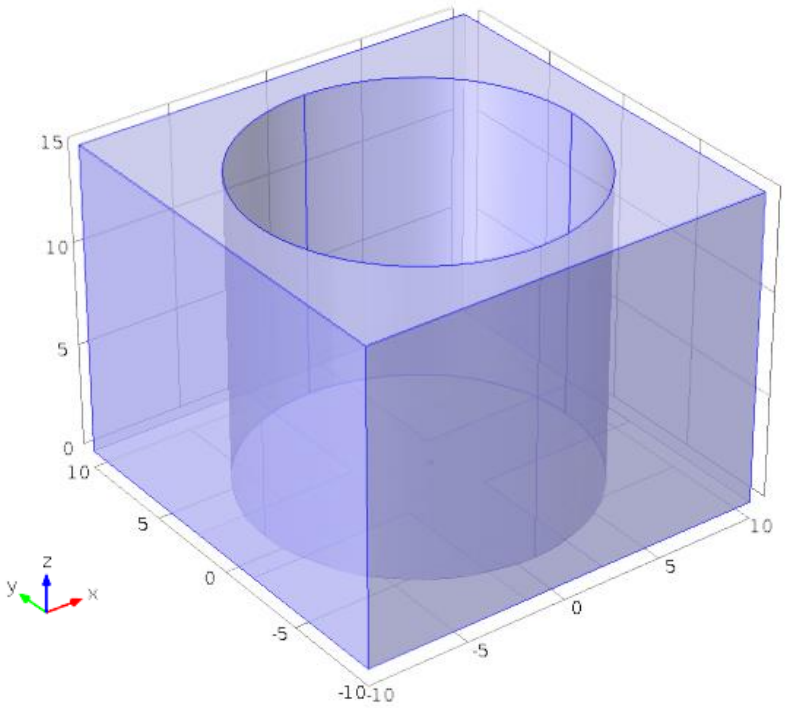

ر. 2-11

Figure 2- 8. Initial concentration in the whole geometry is Zero (C_0=0, except for the vesicle)

The initial condition for the catecholamine concentration at the release site is found as follows. A typical release event contains a total charge of 1pC. Considering that oxidation of each catecholamine molecule transfers two electrons to the electrode, the number of molecules released can be calculated as:

$$number\ of\ molecules = \frac{total\ charge}{q_e q_z}$$

Where, q_e is the fundamental charge of the electron, and q_z is the number of free electrons of each molecule. Hence the total number would be:

$$number\ of\ molecules = \frac{1 \times 10^{-12}}{(1.602 \times 10^{-19})(2)} \approx 3.12 \times 10^{6} molecules$$

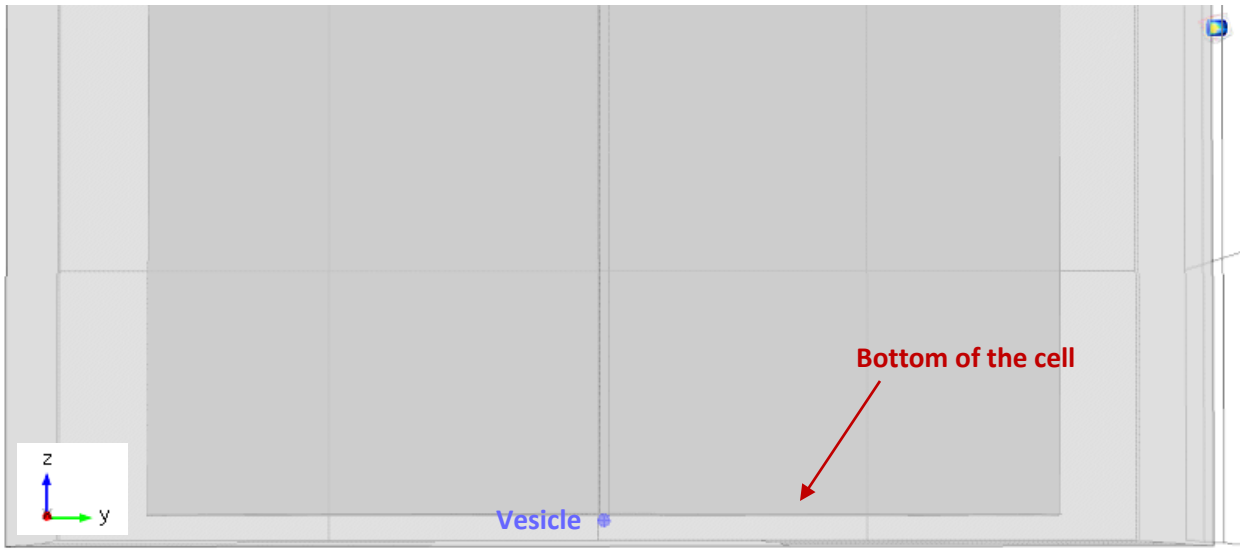

Figure 2- 9. The vesicle is modeled by a sphere with radius of 100nm at (X=1, Y=0.5, Z=0.4) μm.

Since the dimension of the release site in our model is considered as a sphere with radius of 100nm, the concentration of catecholamine molecule can be calculated as:

$$C_{vesicle} = \frac{number\ of\ molecules}{volume \times N_A} \approx 1.24 \times 10^3 \frac{mol}{m^3}$$

Where, $N_A \approx 6.022 \times 10^{23} mol^{-1}$ is the Avogadro number. The vesicle is highlighted as blue in figure 2-11.

Since we have the term $\frac{\partial^2 C}{\partial x^2}$ in the diffusion equation, we need two boundary conditions. In order to solve the time dependent diffusion equation, it is typical to consider the flux boundary condition at different positions in the geometry of the simulation.

The boundary conditions for SU8 walls, bottom and sides of the cell, and the floor of cover-glass are reflecting, i.e., they are impermeable to catecholamines:

$$-n.\nabla C = 0$$

Where, n is the normal vector of the impermeable boundary and C is the concentration (the inner product of the normal vector and concentration is equal to zero). Impermeable boundaries are depicted as dark blue in figure 2-10. The locations of No Flux boundaries are: X=10, *X=-10, Y=10, Y=-10, Z=0,* $X^2+Y^2= (8\ um)^2$ for *Z>300nm* and $X^2+Y^2<(8\ um)^2$ for *Z=300nm)*.

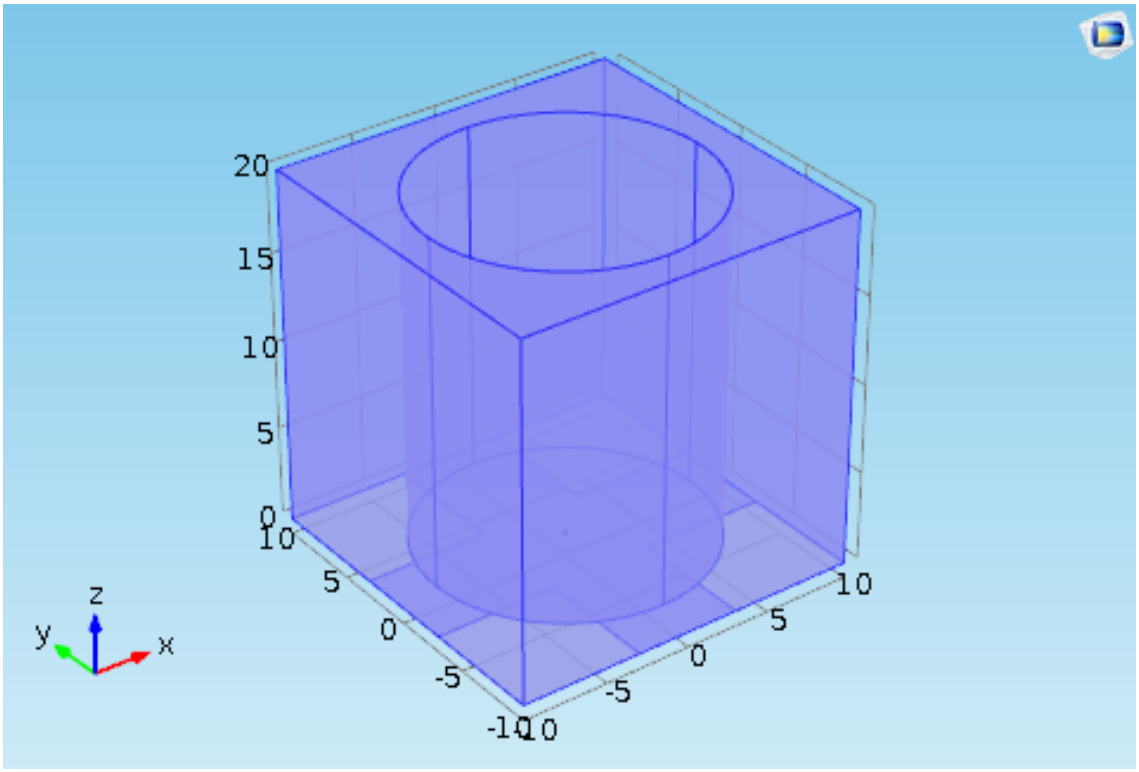

Figure 2- 10. No Flux boundaries are highlighted with dark blue.

Due to the fact that catecholamines get oxidized at the surface of the working electrodes, the boundary condition for all four electrodes is C=0, i.e., all the catecholamine is oxidized on the electrode surface.

2-4-2. Meshing

In FEM the model volume is divided into small and simple geometric forms (Triangles, Tetrahedrals, etc) so that the PDEs can be simplified and then solved numerically. The smaller the meshing size is, the better it can represent model features. In this case however, the simulation will be computationally more expensive. A balance between the resolution and computational speed can be achieved by making the mesh sizes vary throughout the model volume.

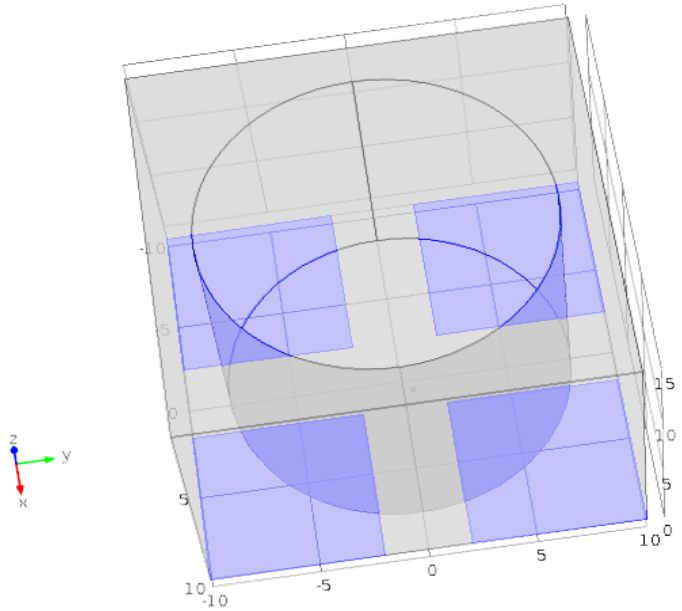

Figure 2- 11. Boundary condition for electrodes (highlighted with blue) is C=0 for any given time.

Regions where concentration gradients tend to be small are assigned larger mesh sizes (Fig. 2-12) whereas regions near abrupt concentration changes or changes in boundary conditions need finer mesh sizes. COMSOL can automatically assign variable mesh sizes, although I found it was necessary to manually set the mesh size very small at the release site because the initial concentration gradient is particularly enormous around this sub-micrometer feature.

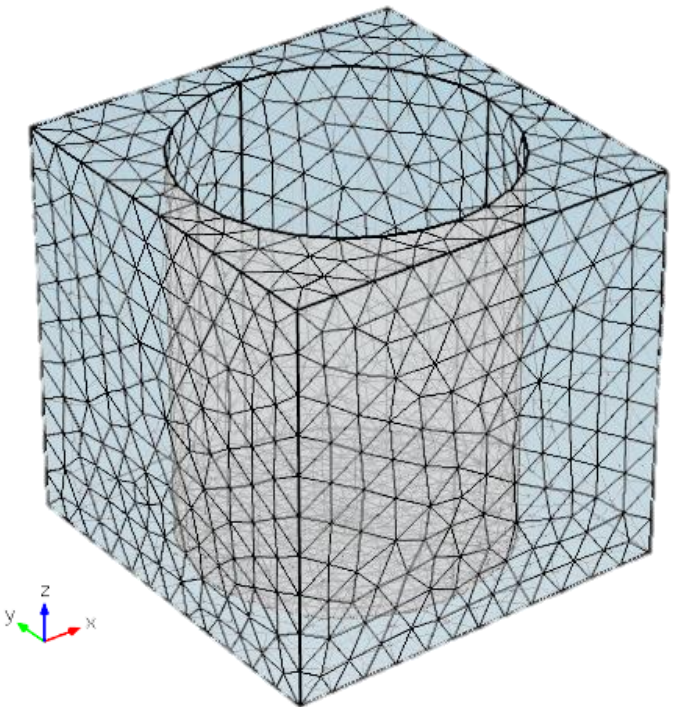

Figure 2- 12. A coarse mesh for the bulk of geometry

Figure 2-12(a) shows meshing of the vesicle with normal meshing size, whereas an extremely fine meshing size which is depicted in figure 2-12(b). It can be clearly seen that with a normal meshing size, COMSOL is not able to resolve the geometry of the vesicle properly.

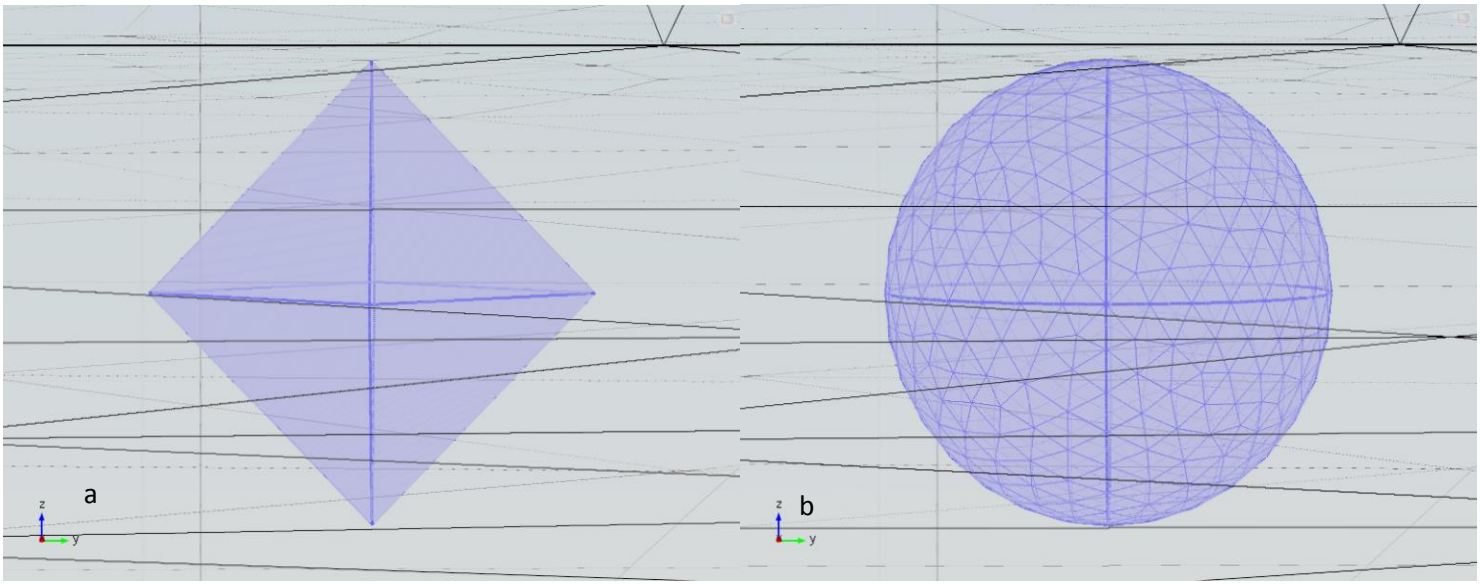

Figure 2- 13. (a) The right hand side depicts the vesicle meshed with a normal size. Whereas (b) the right hand size shows the meshing of the vesicle with an extremely fine meshing size.

2-4-3. Study type

Electrochemical imaging of the release site requires dynamic information about diffusion of catecholamine to each electrode surface, therefore, we have to perform a time dependent study. The simulation was performed over an 800 ms period with time steps of 1 ms.

The position of the release site was moved in a grid pattern at the bottom of the cell between 289 points and a time-dependent simulation was performed at each location.

2-4-4. Simulation result

The data output from the model is the amperometric current recorded at each of the four electrodes. It is possible to monitor the flux rate of any desirable boundary in COMSOL. Since we are interested in the flux of each individual electrode, a boundary probe was defined for each electrode under the definition module. From Fick's second law, it is expected the closest electrode to the release site records the highest flux rate while the furthest electrode from the release site gets the least flux rate. As an example, the release coordinates were defined at (*X=1, Y=0.5, Z=0.5 μm*), and the flux rate of each electrode is shown in Figure 2-13. Electrode3 is the closest electrode to the event (red trace), while electrode1 (blue trace) is the furthest electrode and has the lowest flux rate. The sign convention of flux in COMSOL is as follow: the flux leaving the boundary would be considered as positive while the flux going into the boundary is negative. Therefore, it is important to take this into consideration while we are creating the geometry in order to obtain the correct flux sign.

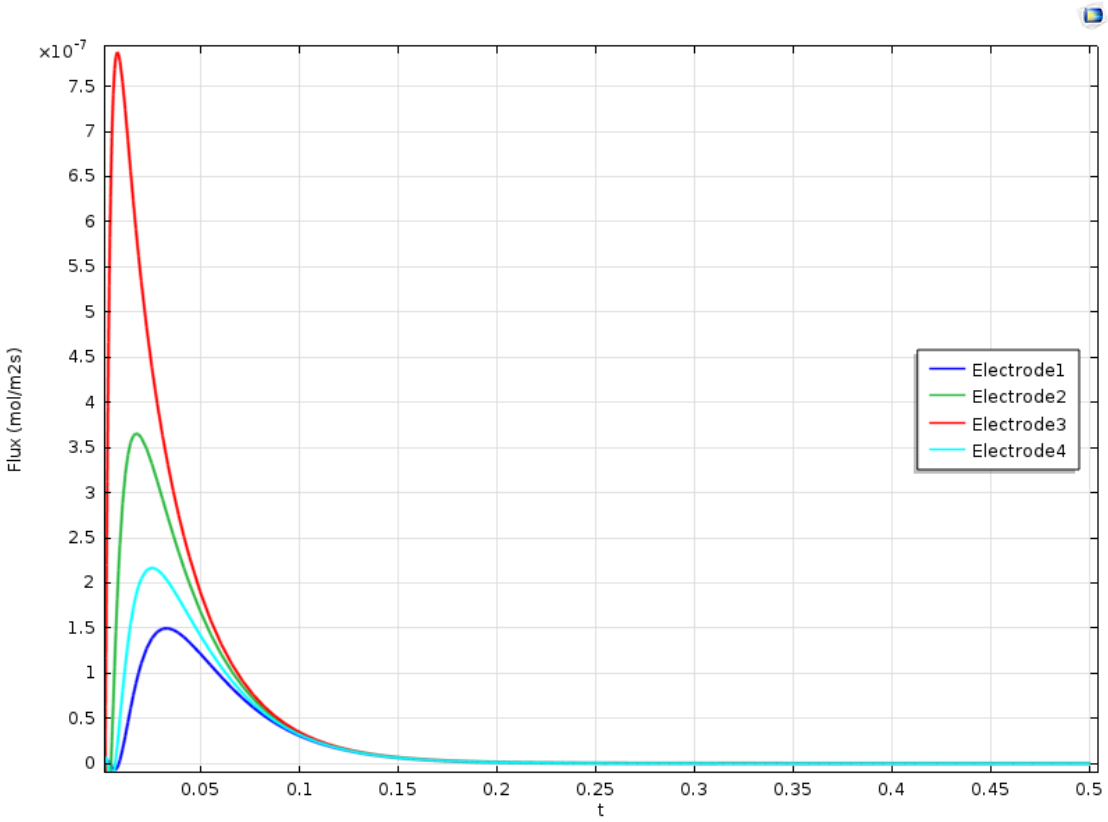

Figure 2- 14. The flux rate through electrode. The red trace shows the flux rate of electrode 3 which is the closes*t* electrode to the event while the dark blue trace shows the flux rate in electrode 1 which is the furthest electrode from the event.

The data obtained from COMSOL simulation are flux versus time, which can be converted to current versus time by applying Eq. 2-12.

$$i = J(\frac{mol}{m^2 s}) \times F(\frac{c}{mole}) \times Z_p \times A(m^2) \qquad \textit{Eq.}\ 2\text{-}12$$

Where, J is the flux rate, F is Faraday constant, Z_p is the number of oxidized electrons of a catecholamine and A is the area of the electrode.

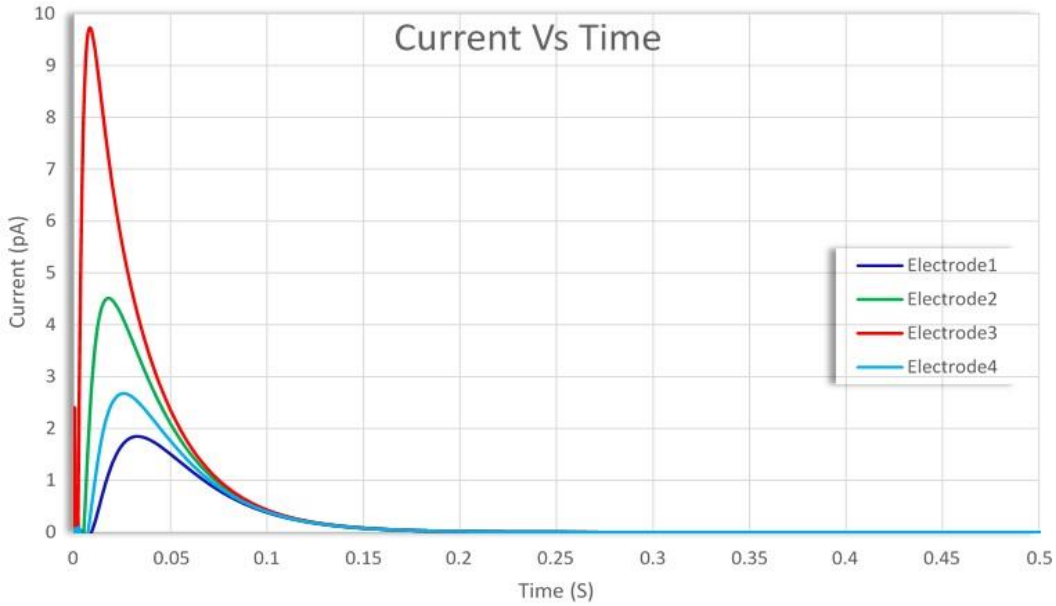

Figure 2- 16. Obtained current from each electrode. Red trace shows the current of electrode3 which is the closest electrode to the event while dark blue trace shows the current of electrode1 which is the furthest electrode to the event.

Clearly if the release site is located exactly at the center of the electrode array, all boundary probes will record the same flux as shown in figure 2-15.

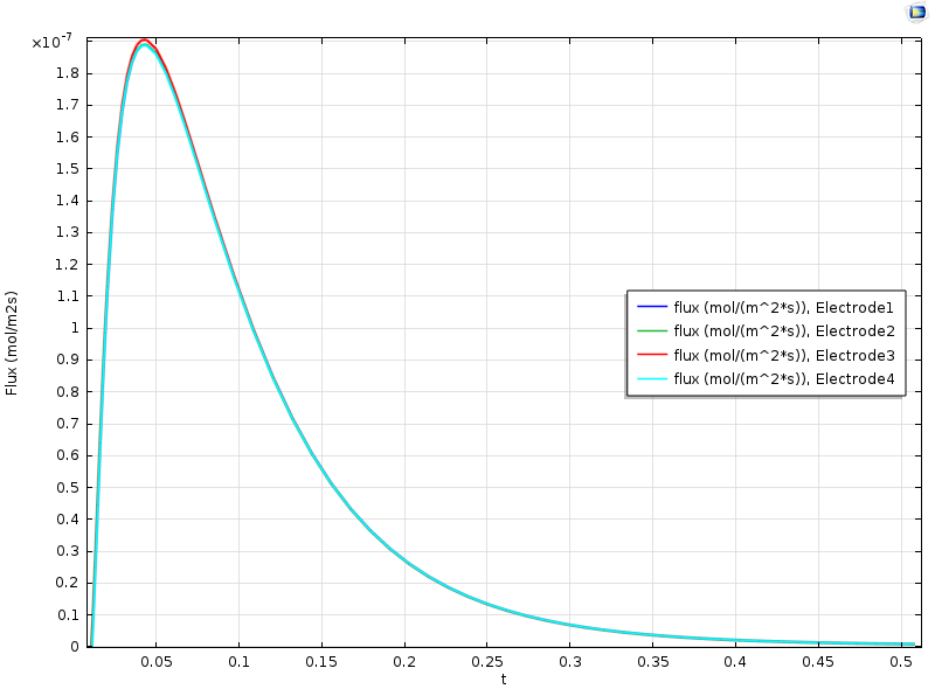

Figure 2- 15. All traces are overlaying each other when the exocytosis event happens exactly at the center. Note that in this graph the electrode size is 7um so that the diffusion delay longer than 8um electrode

2-5. Random walk (Brownian motion)

A random walk consists of successive random steps that leads to a net movement of the particle. For instance, the movement of a molecule in a liquid can be understood by a succession of microscopic random steps. These steps are completely independent from each other so that the future movement of a particle is not dependent on its previous steps. Random walk simulations are used in many different fields such as: physics, chemistry, economics, computer science, biology, etc.

Einstein showed that the movement of particles through a random walk (Brownian motion) is equivalent mathematically to Fick's diffusion law. Therefore, diffusion can be understood, and modeled, as a random walk of particles. The root-mean-square displacement (or standard deviation, σ) of a particle over a time interval t is given by Equation 2-13.

$$\sigma = \sqrt{2nDt} \qquad \textit{Eq.}\ 2\text{-}13$$

Where n is the number of dimension and D is the diffusion coefficient.

So the standard deviation of displacement for a three dimensional diffusion after t seconds is $\sqrt{6Dt}$

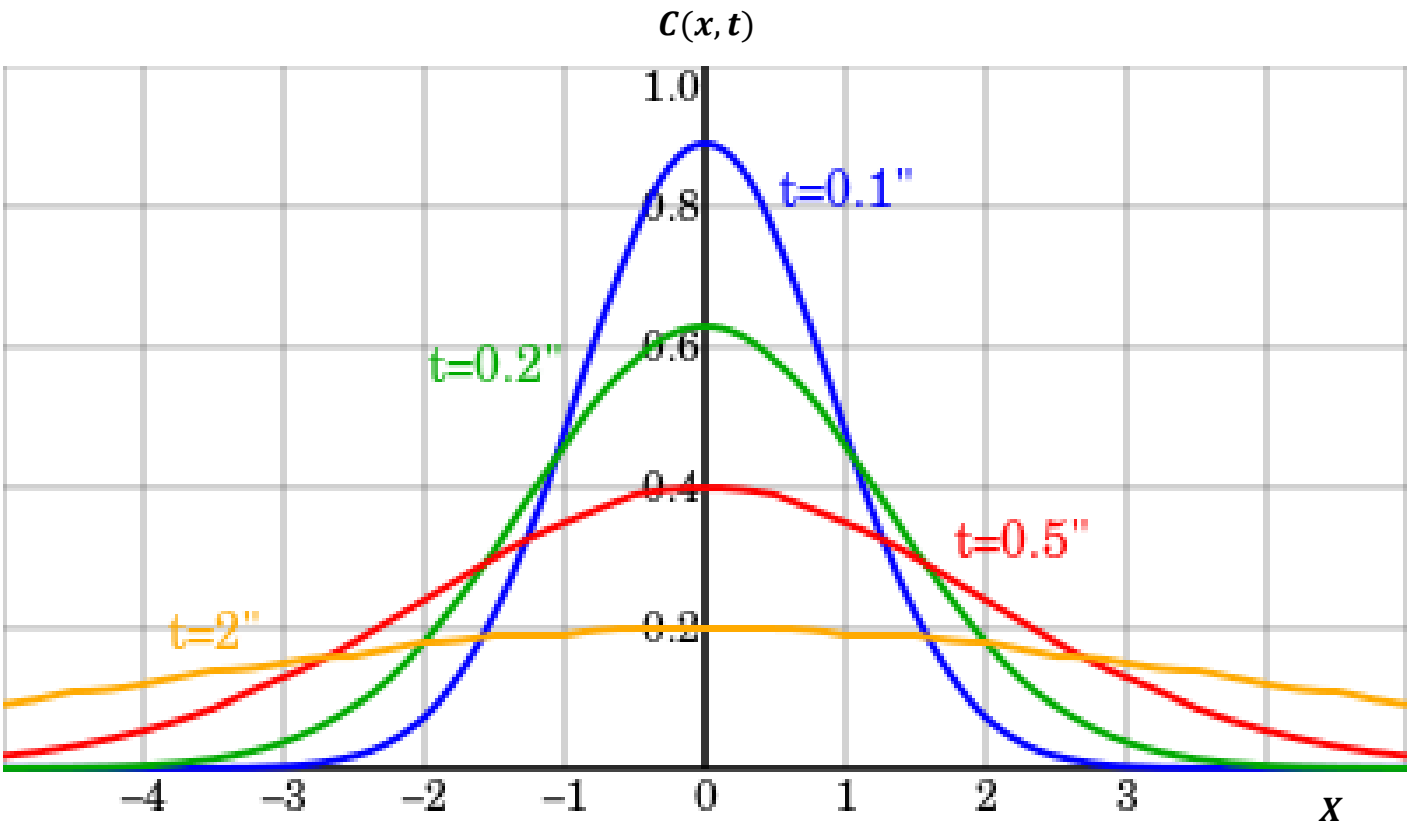

Figure 2- 17. Diffusion profile of a spontaneous release for different time. It can be clearly seen that by passing time the standard deviation of displacement will increase as it is expected. (Image is from Wikipedia)

In figure 2-17, it can be seen that for an instantaneous release (just like what we have in our assumed exocytosis events), the standard deviation of displacement increases with time as it is expected while the concentration gradient decreases.

2-5-1. Random Walk Simulation (RWS)

In order to validate the data obtained from COMSOL, a Random Walk Simulation (RWS) was performed for the geometry of figure 2-10. The simulation was performed

for 20,000 individual particles and the boundary conditions were the same as described for COMSOL simulations.

In order to obtain a relatively smooth flux time course we performed random walk simulations of 20,000 molecules. For each molecule, about 1,000,000 steps are made, with independent step sizes assigned to each direction (x, y and z) by a random number generator with a normal distribution.

2-5-2. Generating random numbers

The simulation is performed for a maximum time of 1 s and the time for each step was set to $1\mu s$. The standard deviation used by the random number generator is given by Eq. 2-11, which is 0.0126 μm for n=1, t=1μs and $D = 8 \times 10^{-5} \frac{\mu m^2}{\mu s}$

A random number is added to the previous position of the particle in each dimension in order to get its new position each microsecond.

2-5-3. Boundary conditions

All boundaries in this RWS were defined and coded through mathematical equations. We have two different types of boundaries. 1. Absorbing (C(x,t)=0) boundaries and 2. Reflecting (No Flux) boundaries.

For each particle random numbers will be generated until either the particle reaches the coordinates of one of the working electrode surfaces (absorbing boundary) or 1,000,000 μs passes from the beginning of the simulation. The time at which the particle reaches a working electrode is recorded and then the particle is discarded from the simulation.

Whenever the coordinates of a particle's location exceeds the coordinates defined for reflecting boundaries, the time and position of the particle will be reset to its previous position and a new random number will be regenerated. Thus the particle is not allowed to pass though reflecting boundaries. This approximation of a reflecting boundary will not affect the simulation results since the time resolution was selected to be very small$(1\mu s)$ which results to a small standard deviation of walking step size $(\sim 0.012\ \mu m)$.

Simulations with 20,000 particles showed that after 500,000 μs about 99.99% of particles got absorbed by electrodes and no particle escaped from the chamber during that time. The final position of all particles are shown by blue dots in figure 2-18.

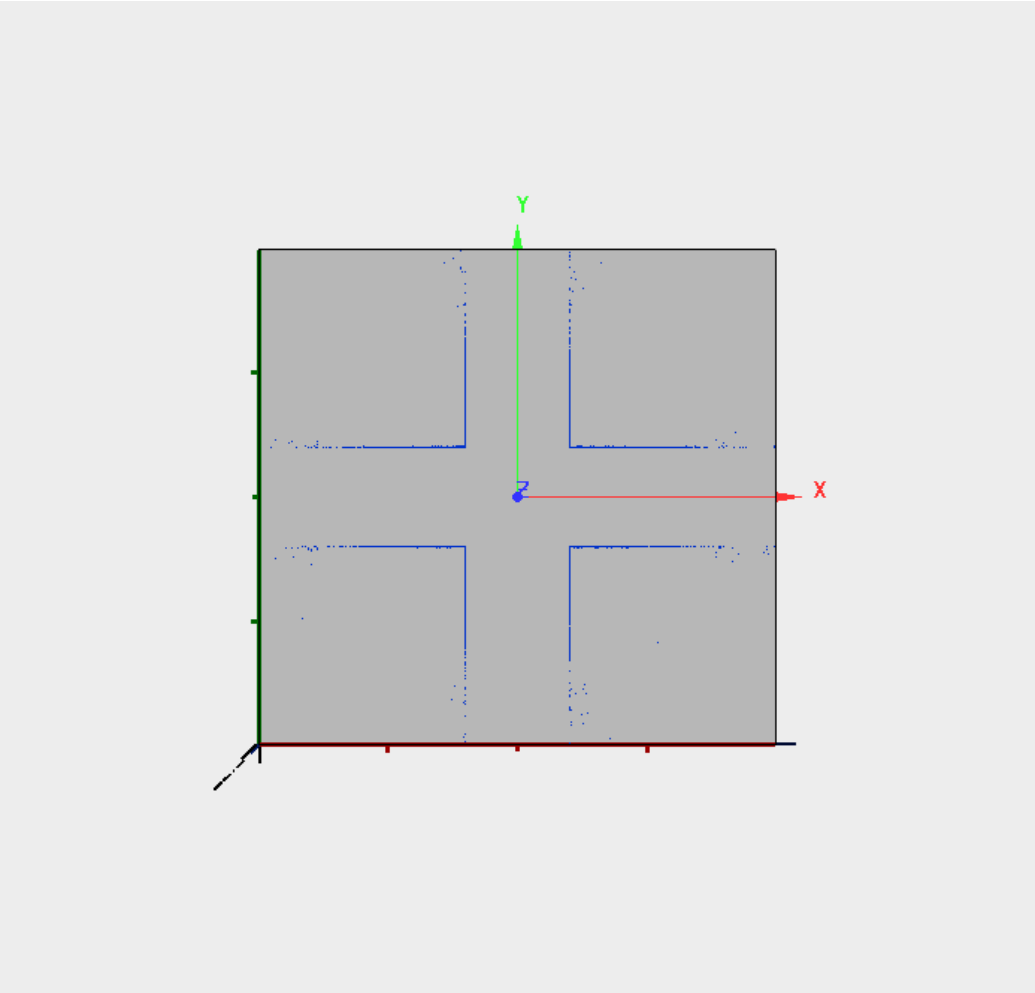

Figure 2- 18. Random Walk Simulation, Final position of the particles.

Figure 2-19 depicts the histogram of particles respect to time. As was mentioned before, a typical vesicle of a bovine chromaffin cell contains about 3.12 million catecholamines, each of which transfers two electrons upon oxidation. Therefore, the ratio of the particles in the simulation (20,000) to the particles in the real vesicle (3.12 e6) is K=156. The current of the simulation can calculated by Eq. 2-15

$$i = \frac{N_p K\, z_p\, q_e}{\Delta t} \qquad \textit{Eq.}\ 2\text{-}15$$

Where, N_p is the number of molecules contacting the electrode over the interval Δt, K is the ratio of simulated molecules to the real number of molecules, $z_p$is the

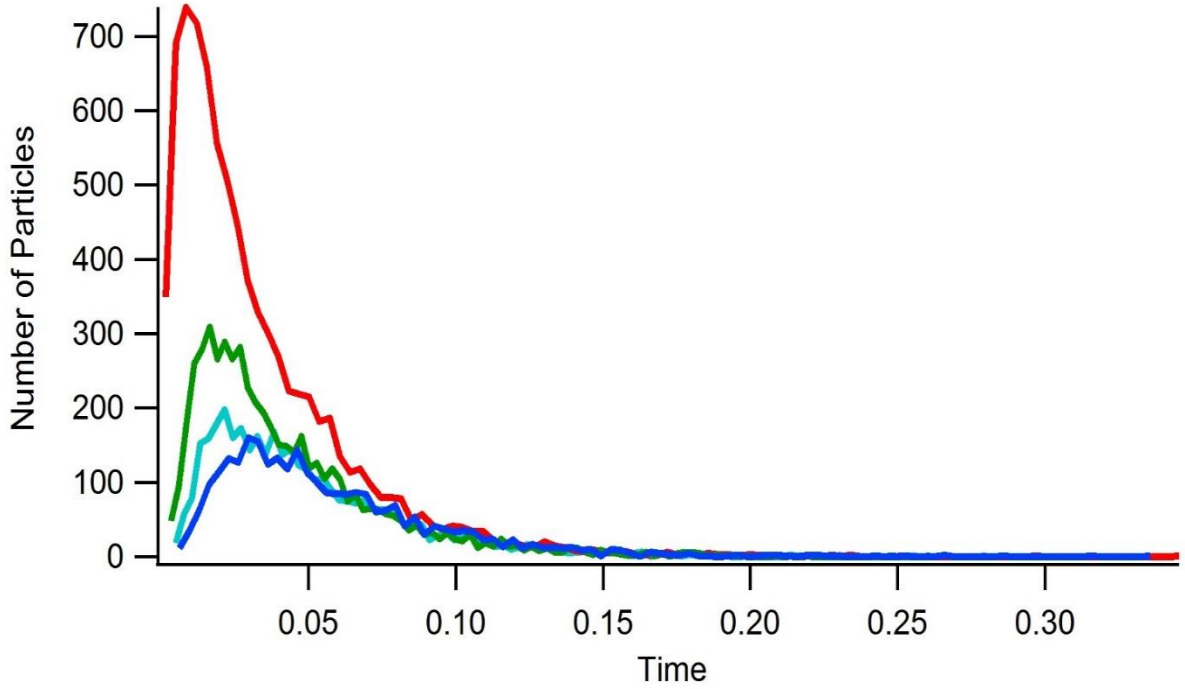

Figure 2- 19. Random Walk Simulation, the number of oxidized molecules for each electrode Vs Time

number of electrons transferred for each molecule and q_e is the fundamental charge of the electron.

Therefore, the current obtained from RWS is shown in Figure 2-20. For the purpose of verifying the results obtained from COMSOL, a Random Walk Simulation (RWS) was coded in Igor Pro. The RWS used the same geometry, initial and boundary conditions used in the COMSOL simulations. The RWS results for all four electrodes were normalized in Igor Pro, as well as results obtained from COMSOL.

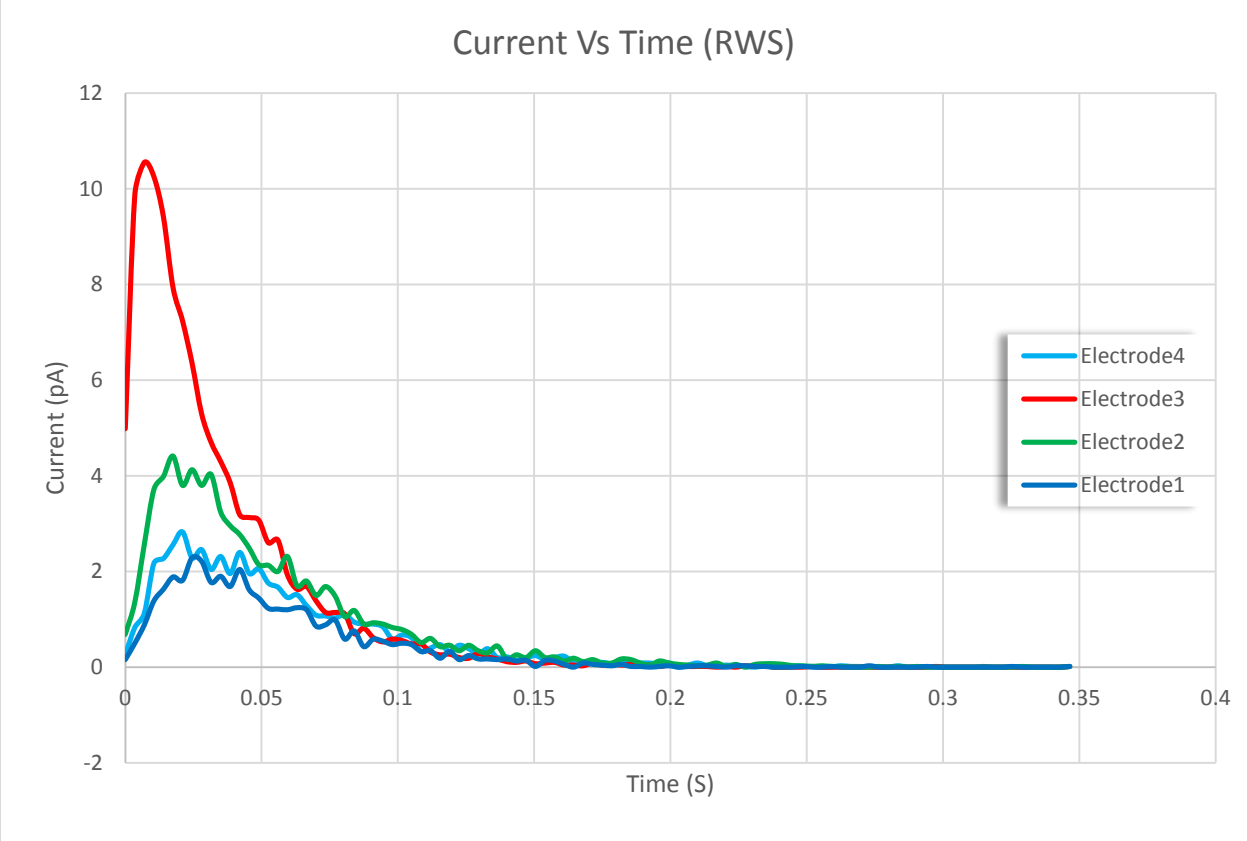

Figure 2- 20. Random Walk Simulation, Current of each electrode Vs Time

Following that both were plotted on the same graph. As it is illustrated in figure 2-21 the normalized results obtained from COMSOL and RWS almost perfectly fit each other.

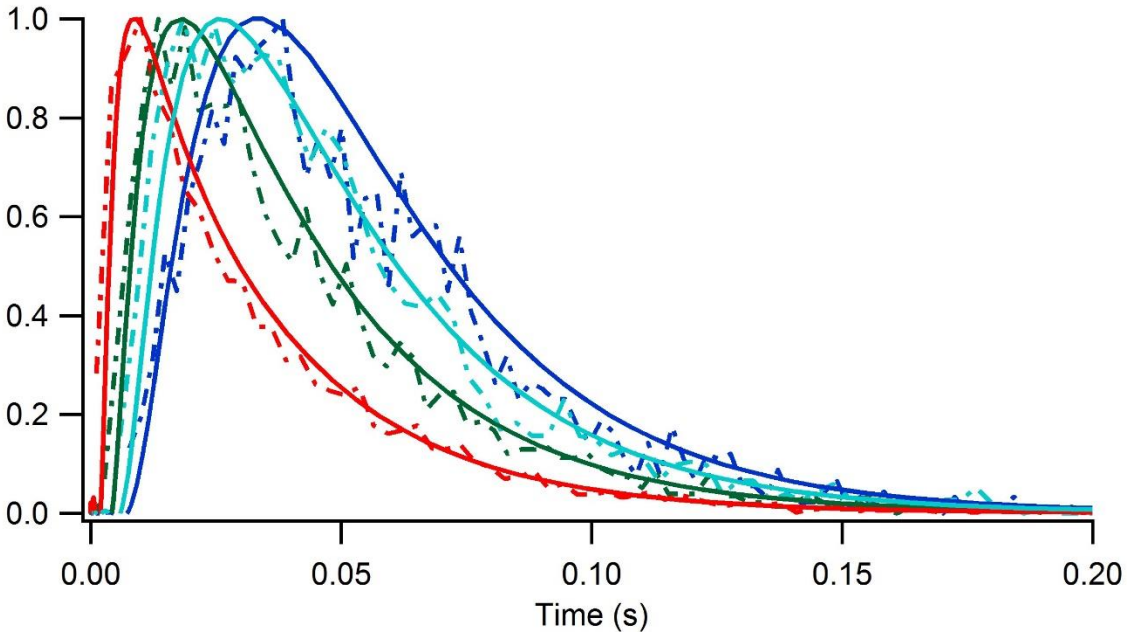

Figure 2- 21. Time Course comparison between RWS (dashed line) and COMSOL (solid line).

Not only the time course of the release in both RWS and FEA are the same, but also the obtained current amplitude is almost the same as well.

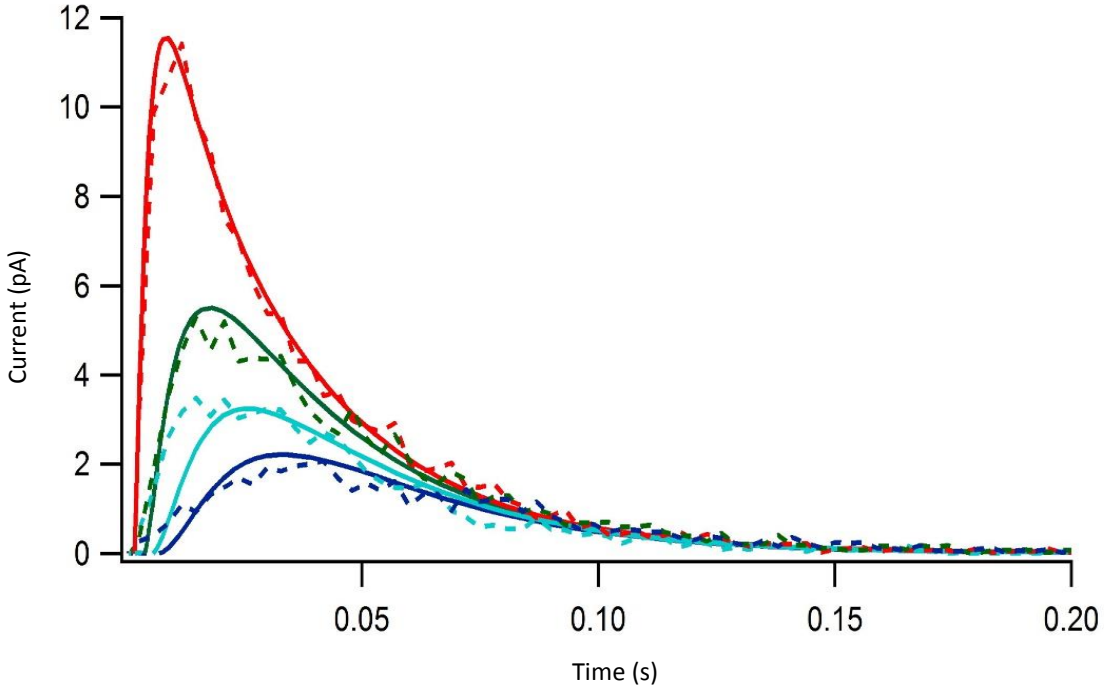

Figure 2- 22. Current amplitude comparison between RWS (dashed line) and COMSOL (solid line).

COMSOL has some advantages over RWS such as:

1. The simulation run for each individual vesicle in COMSOL is about 1 minute Vs. 50 minutes for RWS.
2. Results obtained from COMSOL are smoother than RWS.
3. Due to Graphical User Interface (GUI) in COMSOL it is much easier to make changes in the boundaries in the simulations for future studies.

Chapter III. Materials and Methods

3-1. Introduction

In order to fabricate BioMEMS devices, it is important to choose the materials which are biocompatible so that they don't harm the living cells or tissues. Materials also need to be chosen that are suitable to make up the various components of the microelectrode arrays. This chapter discusses the choice of materials and presents the details of the fabrication process.

3-2. Choice of materials

3-2-1. Substrate and micro-electrode arrays

Due to its transparency and high electrical resistance, glass is an excellent choice for the substrate. However, the glass needs to be very thin (i.e., "cover-glass", ~0.2mm thick) to enable high-resolution fluorescent imaging whereby a high numerical aperture objective lens with very limited working distance is used. Therefore, we used glass coverslips as our substrate.

The working electrodes need to be made from a material which is suitable for electrochemical measurements with fast electron-transfer kinetics, and is low in noise to resolve picoampere currents. In addition, future experiments will employ fluorescent imaging, so a transparent material is desirable.

Indium-Tin-Oxide (ITO) films are very transparent but produce small amperometric signals in response to exocytosis(Kisler, Kim et al. 2012). Diamond-Like-Carbon (DLC) films are semi-transparent, conductive, and suitable for recording exocytosis events(Gao, Chen et al. 2008), but are expensive and not always readily available. Therefore we used gold as the microelectrode material.. It is not as transparent as ITO and is more expensive, but its excellent sensitivity makes it the best choice for these prototyping experiments. Therefore, coverslips were coated with a 30 nm gold thin film on top of a 3 nm titanium adhesion layer prepared at the University of Missouri microfabrication Lab.

3-2-2. Insulation material

A material is needed to insulate the non-working areas of the electrode material that is used to conduct the current signal to connection points at the edge of the chip. Openings in the insulation layer define the working electrodes, which must be of micrometer dimensions to have low enough noise to resolve picoampere-level currents(Yao and Gillis 2012). In addition, a thick insulating material offers the benefit that openings over the working electrodes also serve as microwells to trap a single cell over each working electrode(Liu, Barizuddin et al. 2011). We used SU8 2025 as a thick insulating layer because it is easy to deposit, and is a negative photoresist therefore it is easy to pattern using photolithography.

The biocompatibility of SU8 is not fully known, although it contains heavy metals and solvents that may be toxic to cells(Kotzar, Freas et al. 2002, Nemani, Moodie et al. 2013). Extensive heat curing may make the film much less toxic(Vernekar, Cullen et al. 2009). The experience of the Gillis lab is that cells undergo what appears to be normal exocytosis when cells are acutely (~ 1 hour) placed on devices with SU8 insulating films(Sun and Gillis 2006, Liu, Barizuddin et al. 2011). An alternative thick film is parylene which is known to be biocompatible(Meng and Tai 2005, Chang, Yadav et al. 2007). Although for the first prototype of the device we did not use parylene for patterning the micro-wells, it is a good candidate for future devices.

3-3. Photolithography

Photolithography techniques were employed in the fabrication process of the device. A brief introduction of the fabrication techniques which are used in this study will be discussed before going through the fabrication process.

Photolithography is the most common technique that is used to fabricate mirco/nano scale features in the microfabrication industry. In this process light is used in order to transfer small geometric features through a photomask to a photosensitive material which is called “photoresist”.

There are two classes of photoresist: 1. Positive photoresist and 2. Negative photoresist. As it is depicted in figure 3-1, upon the incidence of light, the negative

photoresist gets polymerized and remains on top of the substrate after development. For positive photoresist however, the unexposed area of the photoresist remains and the exposed area gets depolymerized and will be removed after development.

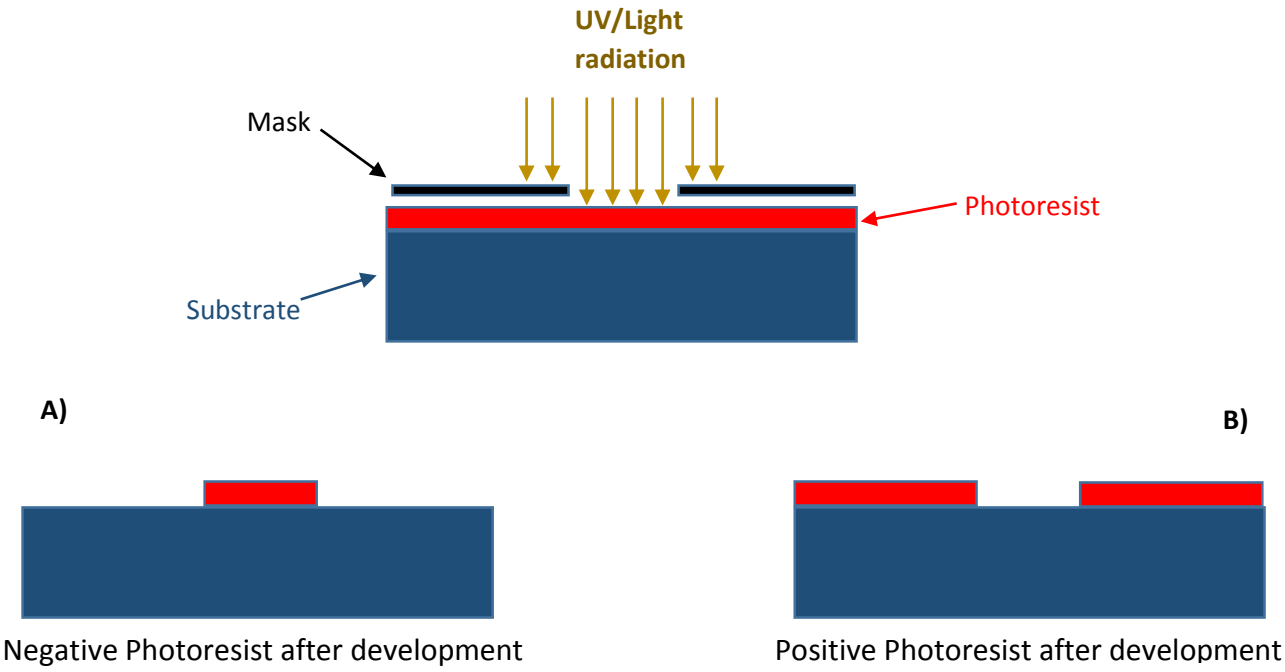

Figure 1-3). The effect of light on positive and negative photoresist. A) Negative photoresist which gets polymerized after exposure. B) Positive photoresist. The exposed area get depolymerized.

Before starting the fabrication process a photomask should be designed and laid out using CAD tools.

The steps of photolithography are sample cleaning, coating photoresist, soft-baking, mask alignment, exposure, post exposure baking, development, post-baking etching, and photoresist stripping (or hard baking).

The first step of micro fabrication is to clean the sample in order to remove any particles, dust, organic or inorganic contaminations from the surface of the substrate. This process is essential in order to precisely transfer the pattern of the photomask on to the photoresist.

Following cleaning, the photoresist must be coated on top of the substrate by means of a spin-coater. The spin rate and the running time of the spin coater can be programmed depending on the viscosity and the desired thickness of the photoresist. Figure 3-2 depicts the spin coater.

Figure 3-2). Spin coater. Depending on the viscosity of the photoresist and the desired thickness, the spin rate and time can be programed through the control panel.

Then, the sample gets heated in order to remove the solvents from the photoresist so that it becomes a solid film. This process is called “soft-baking”. This is a very important step since over soft-baking can leads to a lower sensitivity of the photosensitive material. On the other hand, under soft-baking can prevent light from reaching to the sensitizer which is due to the presence of the solvents.

The next step is UV/light exposure. The wavelength of the exposing electromagnetic wave, numerical aperture of the projection lens, and the resolving capability of the photoresist are the determining factors of the printing resolution. Basically, a smaller wavelength results in a higher resolution, which is why most exposure systems in the semiconductor industry are utilizing UV exposure. The minimum feature size that can be printed can be calculated by Eq. 3-1.

$$R = k_1 \frac{\lambda}{NA} \qquad \text{Eq. 3-1}$$

Where, R is the minimum resolution, $k_1$is constant, λ is the wavelength of the light used NA is the numerical aperture of the projection lens.

Another important factor is the method of exposure. We used contact printing”, where, there is no gap between the surface of the photoresist and the photomask. This results in a more precise pattern transfer since only normally incident light is passed on to the photoresist (Figure. 3-3). A uniform coating of photoresist and

sample cleanliness are important to allow better contact between the photomask and the sample.

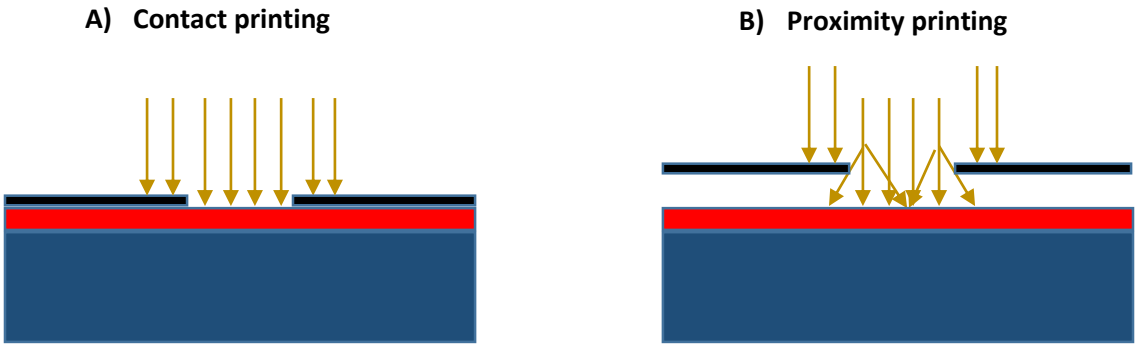

Figure 3-3). Contact printing Vs Proximity printing. A) Contact printing, light doesn't diffract after passing through the photomask. B) Proximity printing, light diffract in the gap between the photomask and photoresist which results in defects in the printed patterns.

The main purpose of the post exposure bake (PEB) of the photoresist is to minimize the effect of the standing waves which are due to the due to the destructive and instructive interference of the incident light. It's been shown that PEB of the photoresist at high temperatures (90-130^{o}C) contributes to the diffusion of the photoactive compound and consequently minimizes the effects of the standing waves phenomena.

Once the PEB is done, we need to wait for a couple of minutes for the sample to cool down. Then, the photoresist must be developed so that the unexposed areas in negative photoresist or exposed areas in positive photoresists will be removed. The result is the transfer of the pattern from photomask to photoresist.

The next step is to post-bake the photoresist which is different from PEB. The purpose of post-baking is to harden the remaining photoresist so that it can withstand the harsh environments like acidic solutions that we use for etching the film on the substrate. It is necessary to keep in mind that post-baking for too long or using too high temperature can result in the flow of the photoresist which leads to the degeneration of the transferred pattern on the photoresist.

There are different methods for transferring the pattern of the photoresist to the substrate such as: etching, selective deposition, or ion implantation. The method that is used in this study is etching (subtractive transfer). In this process the areas of substrate that are not covered by photoresist will be removed by wet etching while the covered areas are protected by photoresist.

After transferring the pattern to the film, the remaining photoresist must be stripped from the sample. There are two major methods for stripping photo resist: 1. Wet stripping by using organic or inorganic solution 2. Dry (plasma) stripping. In this study, a combination of wet and dry stripping was employed in order to remove the remaining photoresist.

3-4. Fabrication process

Before starting the fabrication process we need to design and layout the mask through CAD tools. We need two masks, one for patterning the conductive film and the second mask for patterning the SU8 insulation. As it is depicted in figure 3-4a,

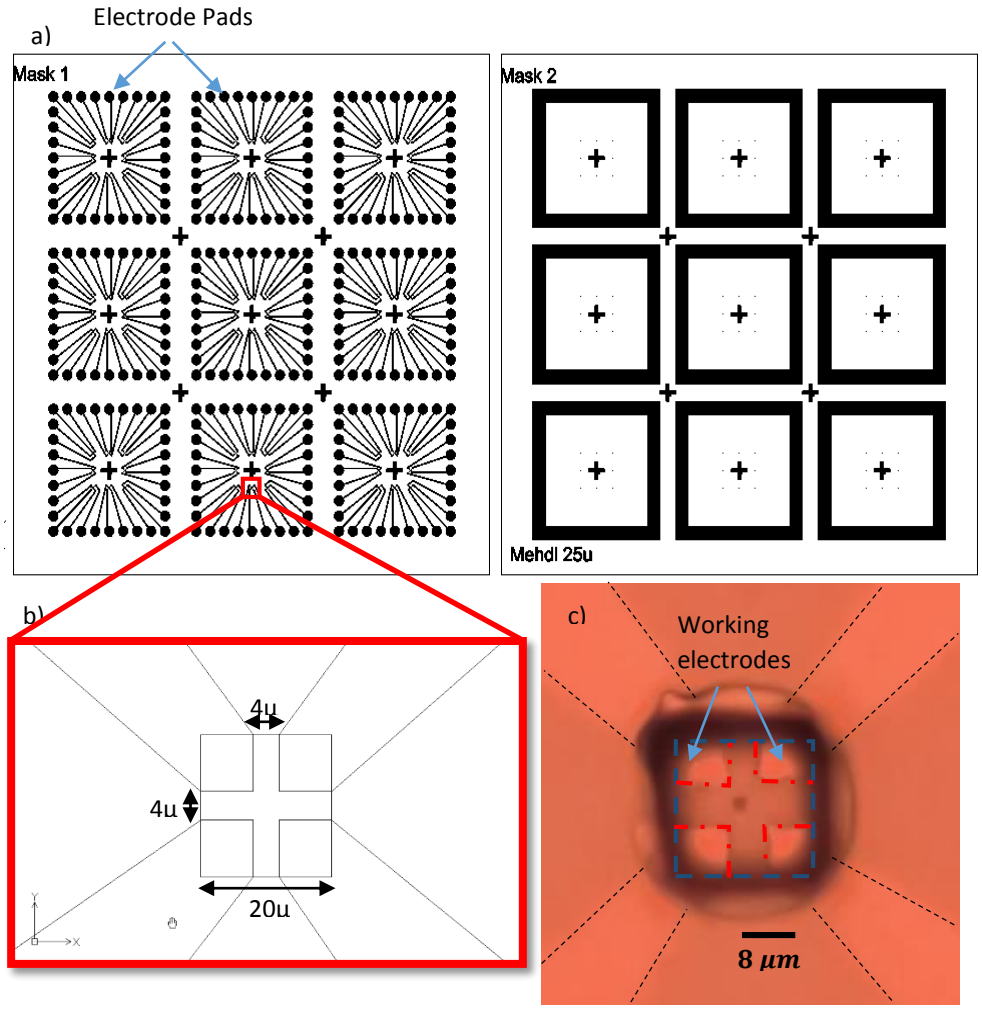

Figure 3-4). a) Mask1 used for patterning electrodes and Mask2 used for patterning the SU8. b) The magnified view of a set of four working electrodes and hole. C) The fabricated device of a set of four working electrodes and hole.

Mask 1 has 9 identical devices, with each device having 32 pads to connect to the amplifier. The 32 recording channels are divided into 8 sets of 4 electrodes with each electrode set recording from one cell. Mask 2 (Fig. 3-4b) has 8 SU8 openings / microwells, one for each cell / electrode set (Fig. 3-4c, d).

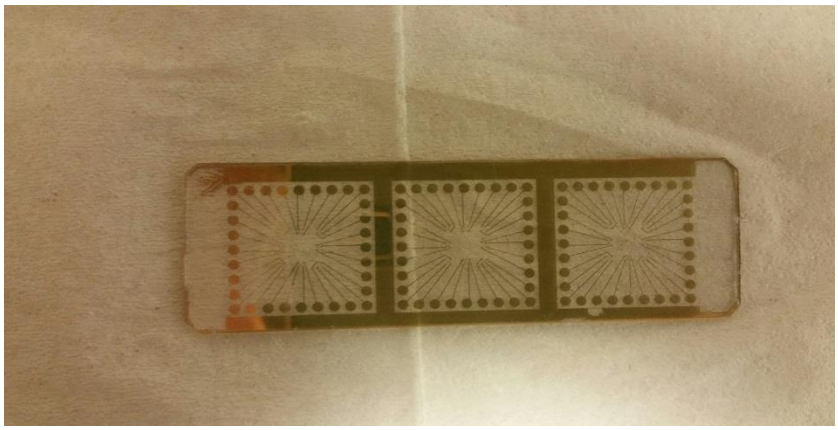

Figure 3-5. Device after patterning the gold film.

a) Cleaning the substrate

The gold film was deposited on top of the coverslip through sputtering in the Microfabrication Lab of the University of Missouri. In order to clean the substrate, the sample was blown with an air gun to eliminate the dust particles and then was immersed in propranolol to remove the organic contaminations from sample followed by rinsing with deionized water (DI water) and drying it with the air gun. Finally, the sample was heated at 65℃ for 4 minutes on a hot plate to dehydrate it.

b) Coating and soft-baking of S1813

4 ml of positive photoresist S1813 was poured and spread out on top of the sample and then spin coating (1. 500 rpm for 10s 2. 2500 rpm for 1 min) was used to result in a film thickness of ~2 μm. Then the sample was soft baked at 115 ℃ for 2 minutes on a hot plate. Before performing the alignment and exposure it is necessary to wait 5 minutes for the sample to cool down otherwise photoresist sticks to the mask and cause inaccuracy in the fabrication process.

c) Exposure, PEB, PB, development of S1813

NuArc 26-1K was used as exposure system. It has a built in light integrator that works with a photo detector in order to compensate voltage fluctuations or any fall off in the light intensity due to the lamp aging. Through the photo detectors the system makes sure that every plate receives the exact light units that is programmed into it. We used 10 units of light for patterning S1813 photoresist. Then, the sample was post baked on a hot plate for 5 minutes at 115℃. S1813 developer was diluted with DI water with the ratio of 1:4 and the sample was immersed in the developing solution for 1 minute to remove the exposed area of the photoresist. The sample was dried with an air gun and post-baked for 2 minutes at 115℃ to harden the photoresist.

Figure 3-5). Electrodes are patterned

d) Etching the gold film

Gold etchant solution also known as “standard aqua regia” (HNO3: HCL, 1:4) was used to pattern the conductive film. The substrate was immersed in the solution for 40 seconds at the room temperature. Subsequently the S1813 film was removed by immersing the substrate in Photoresist stripper 3000 (PRS 3000 from Avantor performance materials) for 5 minutes. Figure 3-5 depicts the result after removing the S1813 photoresist.

e) Coating and soft-baking of SU8

To coat the negative photo resist SU8 and pattern the micro-wells, SU8 2025 was poured on the substrate until it covers approximately 30% of it. Then, it was spin coated at 500 rpm for 10s, followed by 2000 rpm for 22s, then 4000 rpm for 1 minute, yielding a uniform SU8 film with a thickness of $15\mu m$. Then, the sample was put on hotplate and soft baked at 65°C for 3 minutes.

f) Alignment, exposure, PEB, patterning, and hard-baking of SU8

After cooling, the second mask was used to pattern the micro-wells at the center of the four electrode sets. Since the desired resolution of the alignment is less than 1 μm, the Karl Suss MA6 two sided mask aligner was used in order to align the pattern at the center of the four electrode sets (Fig 3-6).

a) b)

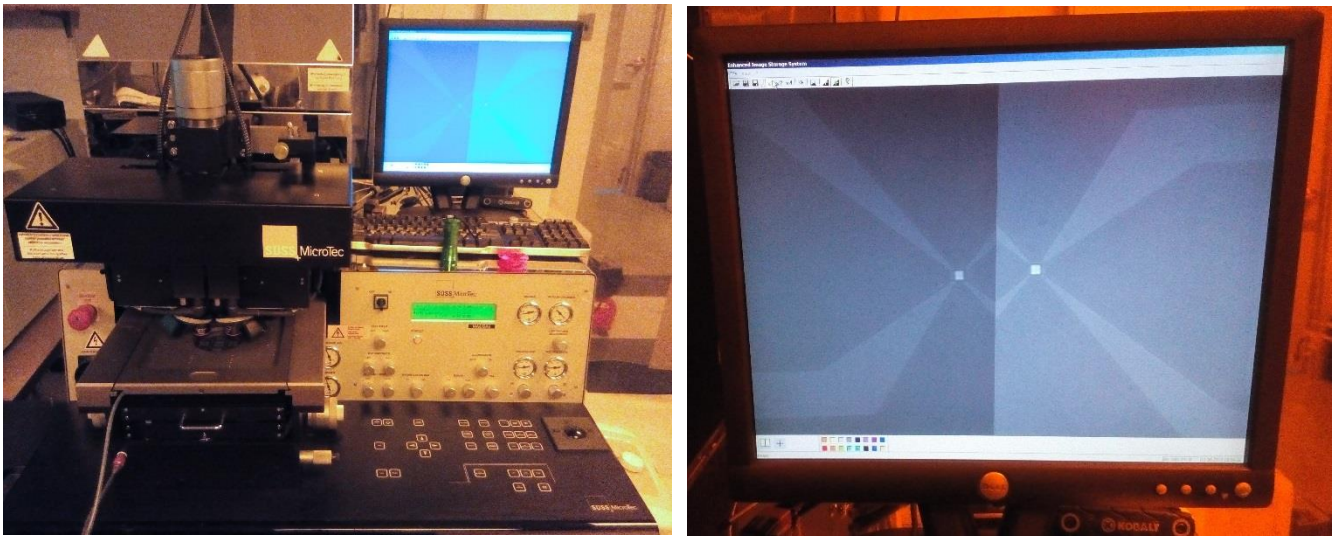

Figure 3-6. a) Karl Suss MA6 two sided mask aligner b) The second mask patterns are aligned at the center of four

UV exposure ($14\frac{mW}{cm^2}$) was applied for 10 s and subsequently the sample was post exposure baked for 5 min on a hot plate. After cooling the SU8 was developed by SU8 developer for 4.75 min then the sample was rinsed with DI water and dried with an air gun. Next, the holes are inspected under a microscope. If the holes are totally opened and properly aligned with the electrodes, hard baking at 180℃ for 10 min is performed in order to harden the patterned SU8 film on the sample.

A brief schematic of the fabrication process is shown if figure 3-7.

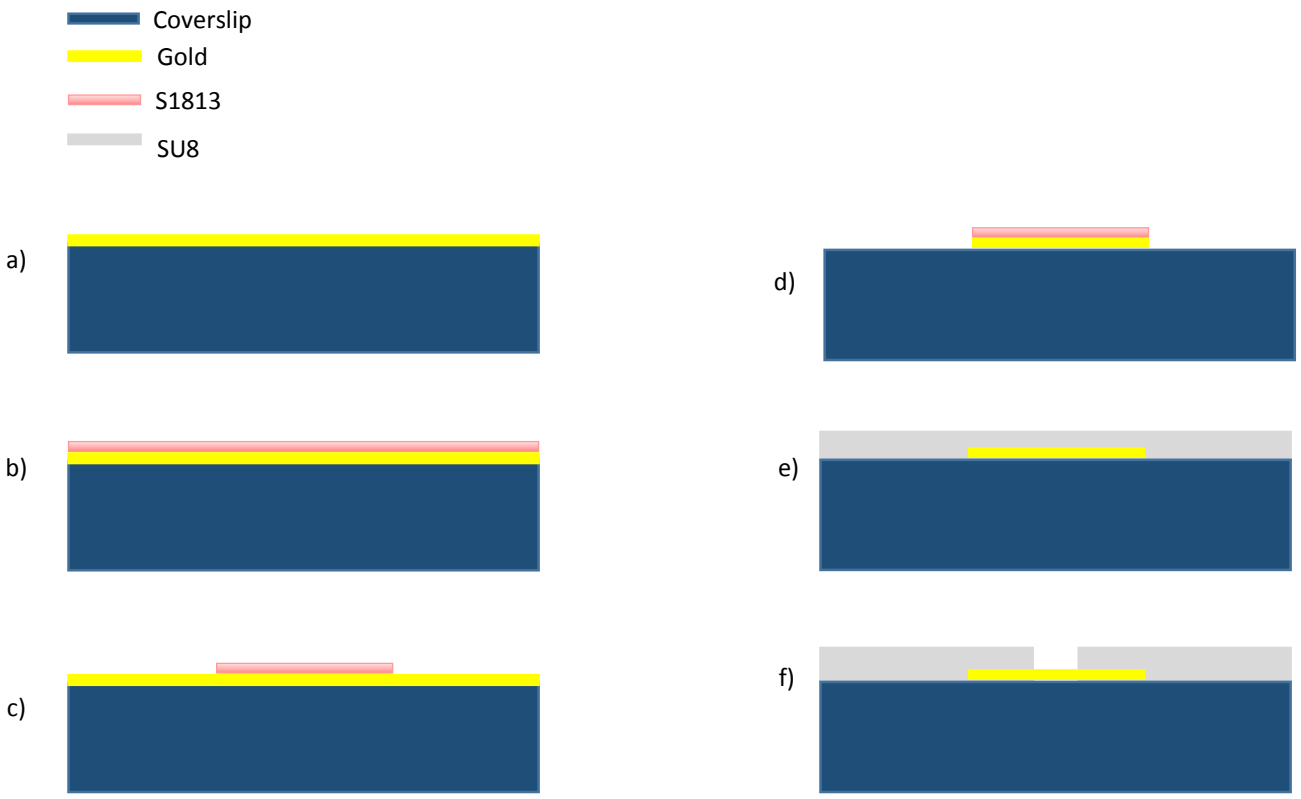

Figure 3-7. a) Cleaning the slide. b) Coating and soft-baking of S1813. c) Exposure, PEB, PB, development of S1813. d) Etching the gold film. e) Coating and prebaking of SU8. f) Alignment, exposure, PEB, patterning, and hard-baking of SU8.

The glass coverglass was diced into separate microchip devices. The glass chips were packaged into cassette devices that serve several purposes: 1. Provide mechanical support to protect the fragile coverglass, 2. Facilitate electrical connection between the connection pads at the edge of the microchip and external amplifiers, and 3. Provide a chamber for holding the cell-containing solution on top of the chip. A small PCB board provided electrical connections to the pads on the chip using conductive epoxy whereas a standard header array on the PCB facilitated connection of the 32

channels to the amplifier. A chamber was fabricated with a 3D printer and bonded to the microchip and PCB using superglue to make a water-tight seal.

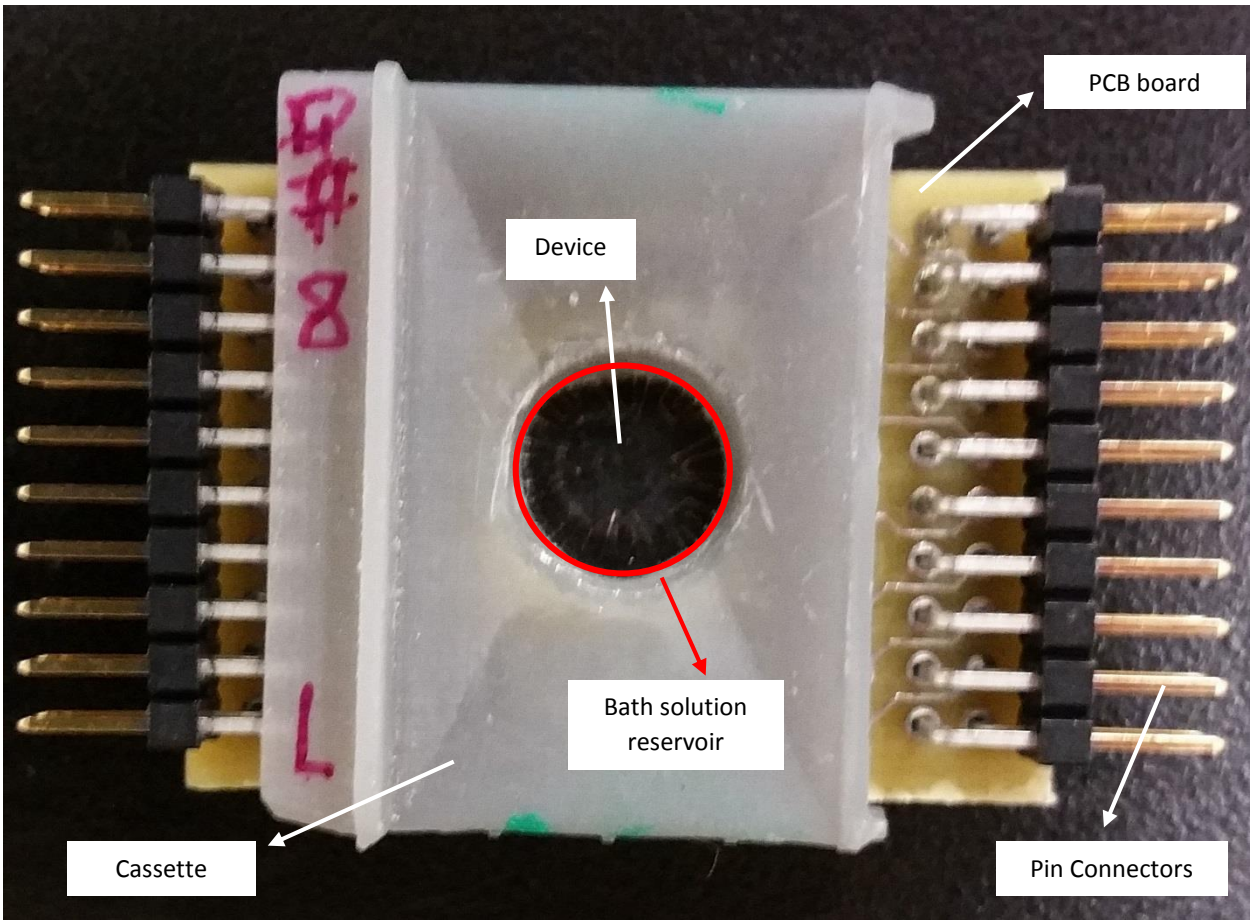

Figure 3-8. The device is mounted and leak proofed to the cassette and PCB board.

Figure 3-8 depicts the device which is ready to be connected to the amplifier head stage, the bath solution and cells are added to the fluid chamber which is highlighted in figure 3-8 with a red circle.

3-5. Cell preparation

Chromaffin cells were isolated from bovine adrenal glands (Hamill, Marty et al. 1981, Ashery, Betz et al. 1999, Yang, Craig et al. 2007) and kept in a culture in a humidified incubator at 37^{o}c for 5 days in culture flasks in Dulbecco's Modified Eagles Medium supplemented with 10% (v/v) fetal bovine serum and 1% penicillin/streptomycin in a refrigerator for up to 5 days. The bath solution consisted of (in mM): 150 NaCl, 5 KCl, 2 CaCl2, 1.2 MgCl2, 10 HEPES, and 11 glucose, pH 7.2.

In preparation for an experiment, cells were detached from the flask with a vigorous wash of culture media and then centrifuged at 100g for 4 min. The supernatant was removed, and the cells were suspended in 5mL of standard bath solution followed by a second pelleting. The supernatant was again removed, and the cells were resuspended in 1mL of standard bathing solution, resulting in a typical cell density of $\sim$2x10^{6} cells/mL. We loaded 50 µL of the cell solution in to the reservoir of the microchip device and waited for 15 min to allow the cells to settle. Exocytosis was triggered immediately following the wash by adding 100 µL of the "high-K^{+}" solution, consisting of 55 NaCl, 100 KCl, 5 CaCl2, 2 MgCl2, 10 HEPES, and 10 glucose, titrated to pH 7.2 with KOH (all in mM)(Liu, Barizuddin et al. 2011).

Chapter IV. Result and discussion

4-1. Electrochemical testing of device

Even with the best fabrication process, there might be some electrodes that are not working as expected. Therefore, it is recommended to test the microelectrodes before loading cells and doing the actual recording. This helps us to know that which electrodes are expected to record current. Cyclic voltammetry (CV) using the Ferricyanide/Ferrocyanide redox couple is a popular technique to identify the working electrodes that have sufficient sensitivity to be used for cell studies.

4-1-1. Introduction to Cyclic Voltammetry (CV)

Cyclic voltammetry (CV) is a technique in electrochemistry that reports the reduction and oxidation of an analyte on the surface of a working electrode. In this technique, a ramp in potential is applied to a working electrode with respect to a reference electrode (e.g. Ag/AgCl). Then, the voltage is scanned in the reverse direction to complete the cycle. The current recorded from the working electrode is plotted versus the applied voltage in order to obtain the so-called 'cyclic voltammogram' graph (figure 4-1). This graph contains information that can be used to analyze the properties of the analyte or/and electrodes. When the voltage is ramped in the negative direction, the electrodes reduce the analyte and results in a cathodic current. This cathodic current increases and reaches a peak value ($i_{p,c}$) and then

decreases. This is due to the fact that the analyte get consumed and its concentration decreases in the proximity of the working electrodes, which eventually results in a current limited by the rate of diffusion. When the voltage is ramped in the positive direction, the working electrode oxidizes the analyte, resulting in an anodic current with an anodic peak value ($i_{p,a}$) that declines due to consumption of the analyte (figure 4-1 b).

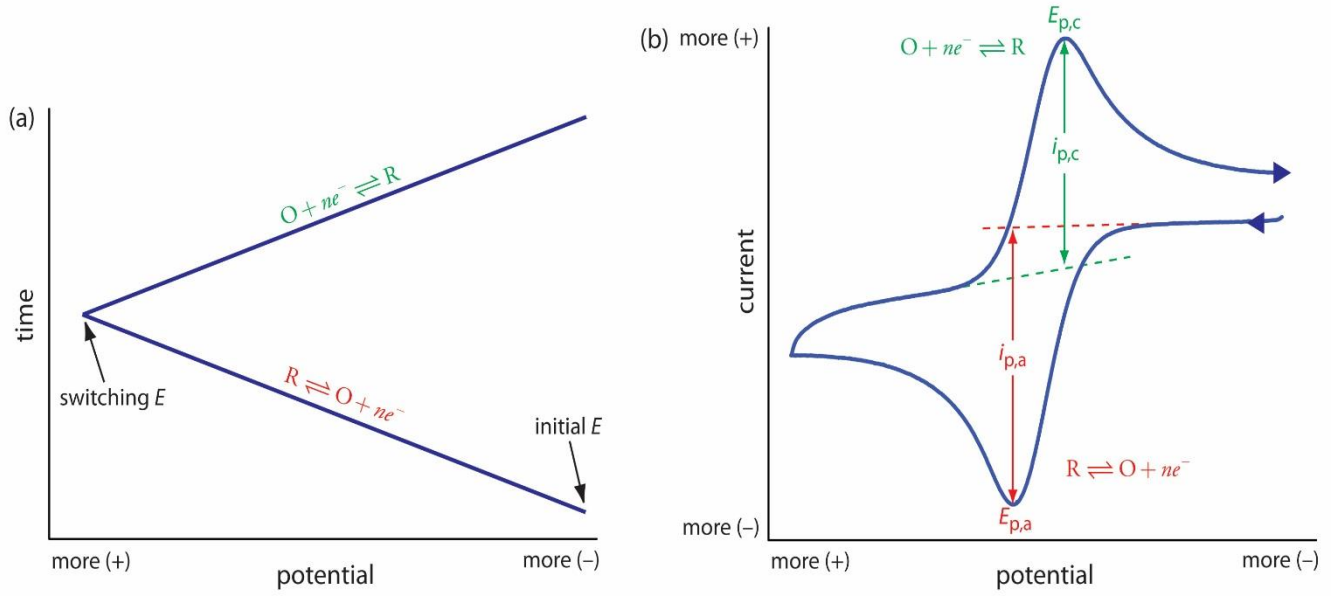

Figure 4-1. a) The scanning potential. b) Voltammogram obtained from a CV (From ChemiWiki)

Ferrocyanide/ Ferricyanide is often used as a test analyte because it is a readily reversible redox couple without side reactions (Eq.4-1).

$$Fe(CN)_6^{-4} \leftrightarrows Fe(CN)_6^{-3} + e \qquad \text{Eq.4-1}$$

Equation 4-1 describes the reversible oxidation of ferrocyanide.

Features that verify the sensitivity of the electrode is that the transition to the cathodic current is steeply dependent on voltage, occurs near the expected potential (~0.15 V for ferricyanide), and reaches a peak value. The value of the peak current, in turn, indicates that the electrode is the expected size. In contrast, electrodes with poor sensitivity (e.g., are dirty) often show a shallow transition in current that never reaches a plateau and very large or small currents indicate improperly insulated or partially covered electrodes, respectively.

4-1-2. Analytical solution of the diffusion-limited current for a test analyte

The theoretical value of the diffusion-limited cathodic current for a disk electrode surrounded by an insulating (reflecting) barrier of infinite dimensions can be calculated by solving the diffusion equation as(Anderson 2001):

$$i_{lim} = 4nFDCr \quad \text{Eq.4-2}$$

Where n is the number of electrons transferred per molecule (1 for Ferricyanide), F is faraday's constant, D is the diffusion coefficient ($7.2 \times 10^{-10} \frac{m^2}{s}$), C in the concentration of analyte (here 1 mM), and r is the radius of the disk electrode.

However, our situation differs: 1. there are four square electrodes instead of one disk electrode, 2. The 15 um thickness of the SU8 film will affect the diffusion profile.

Therefore I carried out FEA simulations in order to predict the current we expect for functional electrodes in experiments with a test analyte.

4-1-3. COMSOL simulations of chronoamperometric current to solve for the diffusion-limited current in a test analyte.

My goal for the simulations was to determine the expected diffusion-limited cathodic current for our electrode geometry. However, simulating the reaction-diffusion process during cyclic voltammetry is quite complicated, so I performed the simulations for the simpler chronoamperometry experiment. With chronoamperometry the voltage is stepped from a voltage that does not support the electrochemical reaction to one that allows the electron-transfer reaction to occur rapidly on the electrode surface so that diffusion of the analyte is the rate-limiting step. In the simulations this corresponds to having an initial condition whereby the concentration of the analyte is uniform, whereas after the step a boundary condition is imposed that the concentration on the electrode surface is zero, whereas the concentration far from the electrode remains the same as the initial condition. The results of the simulation are depicted in figure 4-2. The cathodic current rapidly decays in the initial seconds as the concentration of ferricyanide near the electrode rapidly declines, producing a "depletion layer". After the initial transient, the current reaches a nearly constant pseudo-steady-state value limited by diffusion of ferricyanide into the depletion layer. As can be seen in the figure 4-2, the

approximate diffusion-limited current for each electrode in 1 mM ferricyanide is ~0.3 nA.

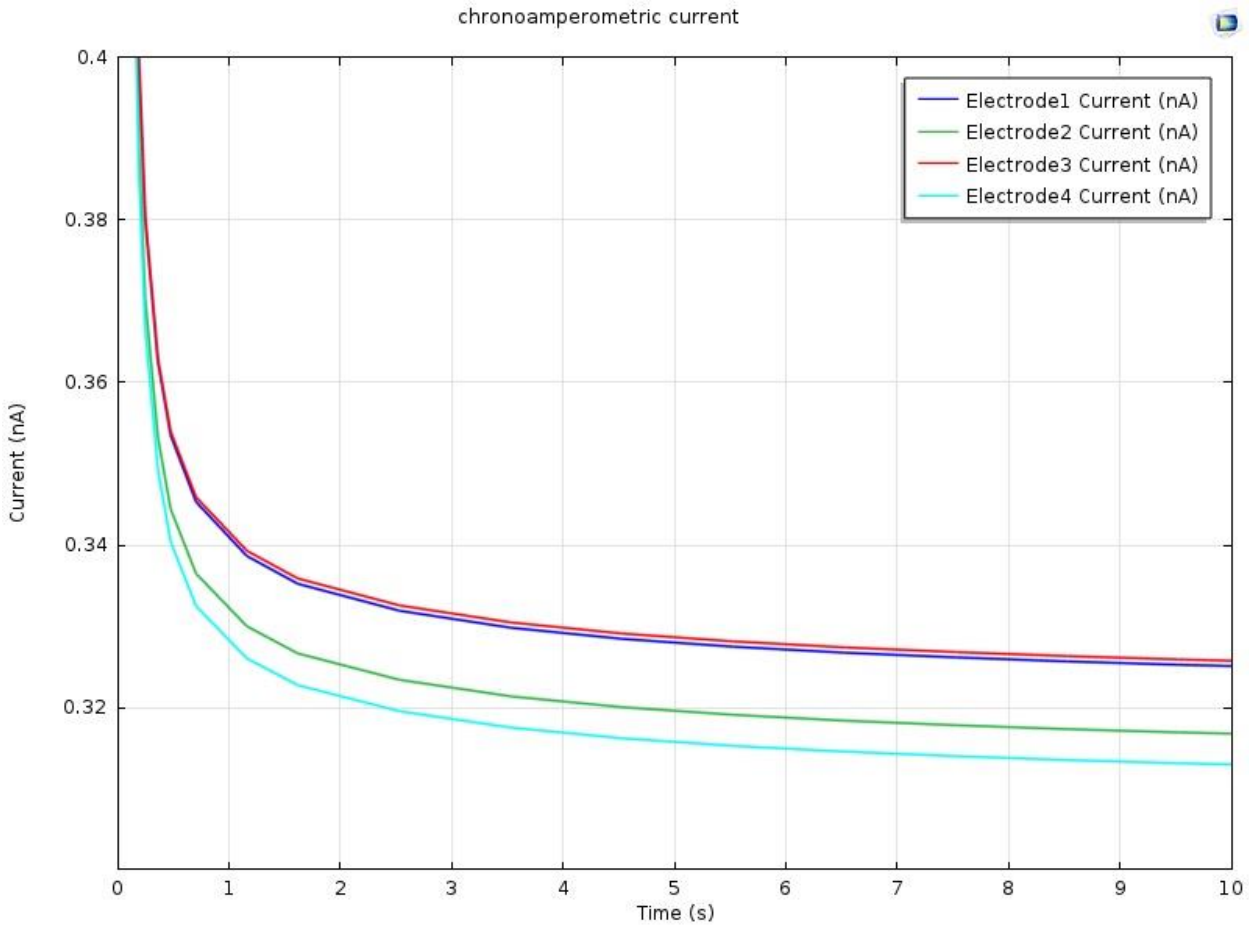

Figure 4-2. Chromo-amperometery for 1 mMol Ferricyanide, 8X8 μm square electrodes, and with a SU8 microwell with a dimension of $20 \times 20 \times 15\ \mu m$ $(L \times W \times H)$

4-1-4. Experimental CVs

Before performing the CV, the device was treated with air plasma for two minutes to clean the electrodes, including removing any SU8 residue on the surface (Figure4-3).

About 0.1mL of 1 mM ferrocyanide solution was placed in the reservoir of the device and the reference Ag/AgCl electrode was immersed in the solution.

As is shown in figure 4-4, the 32 electrodes of the device were connected to two different amplifiers (D1, and D2, each of which had 16 channels). Since each amplifier has 16 channels, CVs for all electrodes can be done simultaneously.

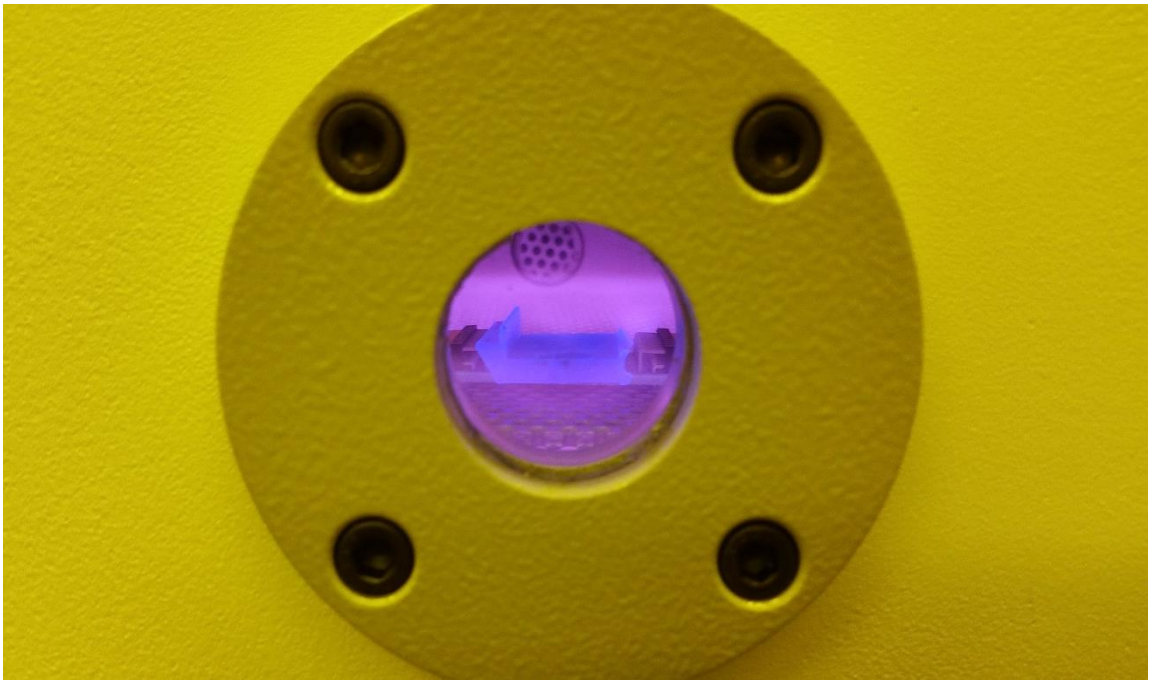

Figure 4-3. Air plasma treatment for removing residual SU8 and other organic contaminants.

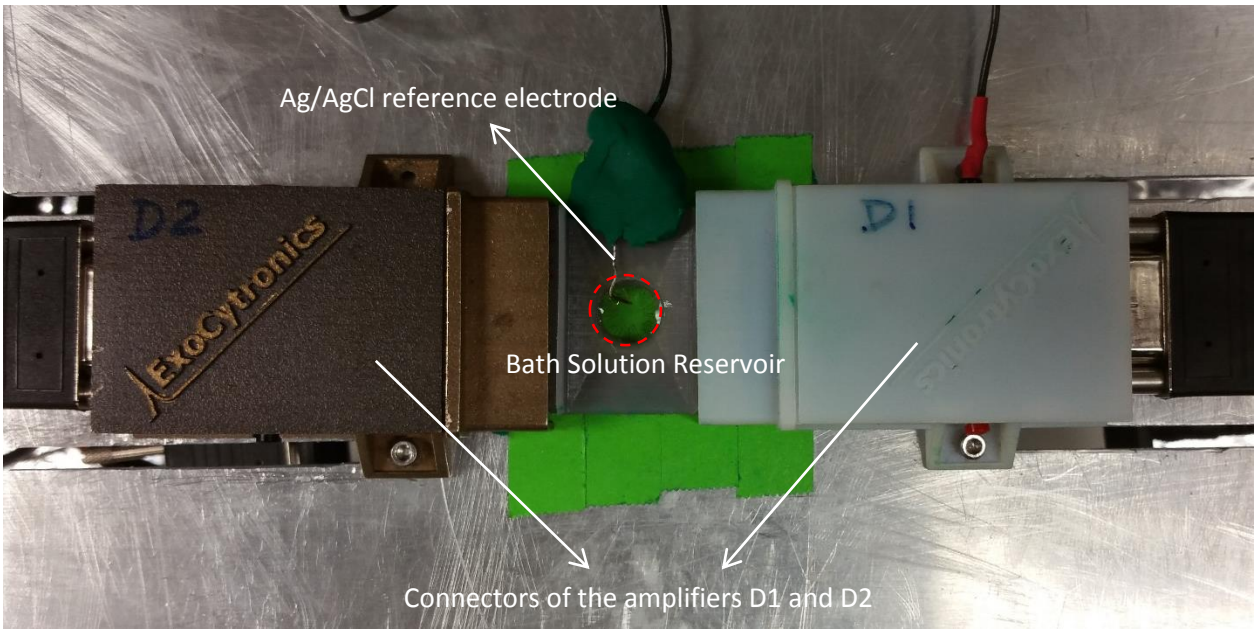

Figure 4-4. Setting up the amplifier for CV recording. The dashed re circle is depicts the device reservoir.

Figure 4-5 presents the CVs obtained from one microwell device with four electrodes. The voltage is swept from +0.5 to -0.5 volt at a scan rate of 10 mV/s. The 4th electrode could not be recorded due to the malfunctioning of channel 13 of amplifier D1. Contrary to theory, the response varies between the three electrodes that were measured. A logical explanation for the differences in current is that the electrodes do not have identical areas because the microwell is not exactly centered over the four electrodes. Note, however, that the diffusion-limited currents are of the appropriate order of magnitude predicted from the FEA simulation. Also, the shapes of the three CVs are appropriate, with a sharp transition to the cathodic current at an appropriate potential, and a clear plateau current. Therefore we expect these electrodes show the expected sensitivity for cell recordings of exocytosis.

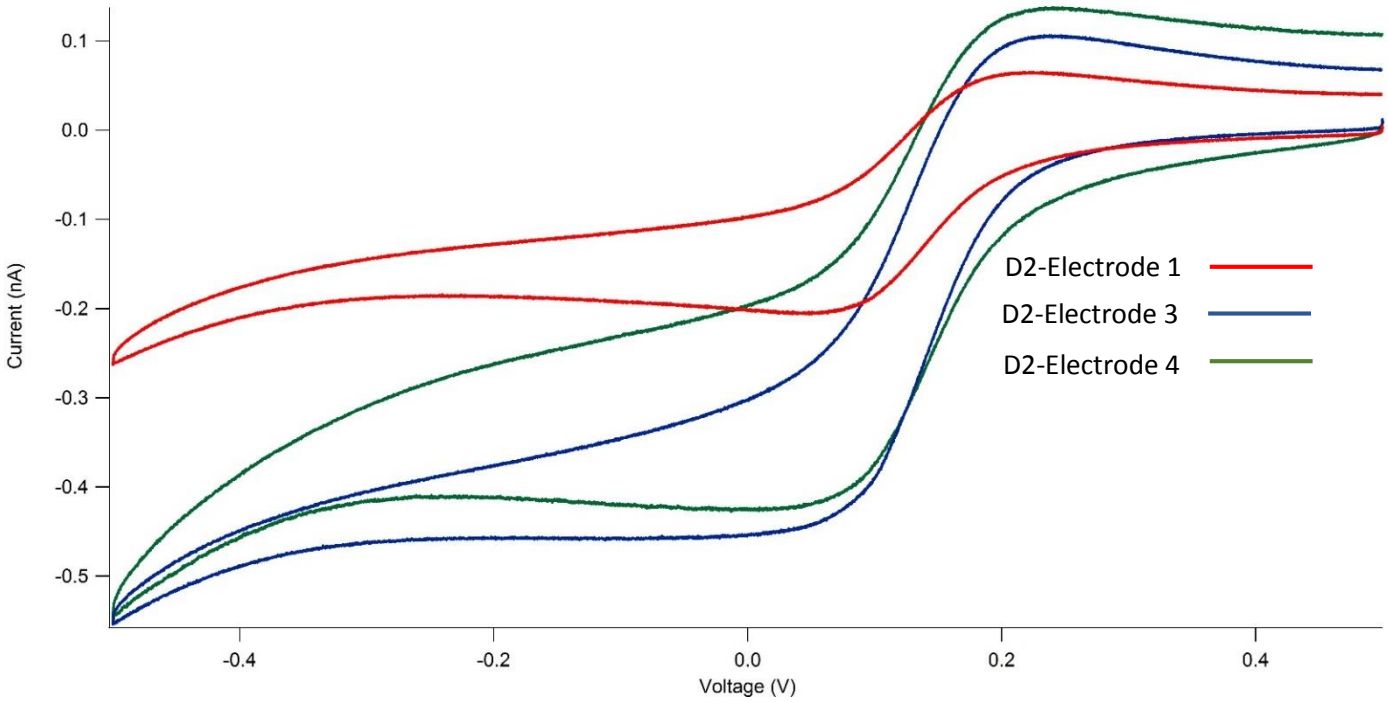

Figure 4-5. Cyclic voltammetry of electrodes 1, 3, and 4.

4-2. Amperometeric cell recordings

Immediately prior to performing amperometeric cell experiments, the device was treated with air plasma in order to remove organic residues from the surface of the microelectrodes. Subsequently, the electrodes were coated with poly (L-lysine) (PLL) in order to promote cell adhesion (Liu, Barizuddin et al. 2011).

A 100 μl drop of solution containing bovine chromaffin cells at a density of ~ 2×10^6 cells/mL was placed on the reservoir and the cells were allowed to settle for 10 minutes.

Figure 4-6 depicts a sample photomicrograph of a cell trapped in a microwell on top of the four electrodes.

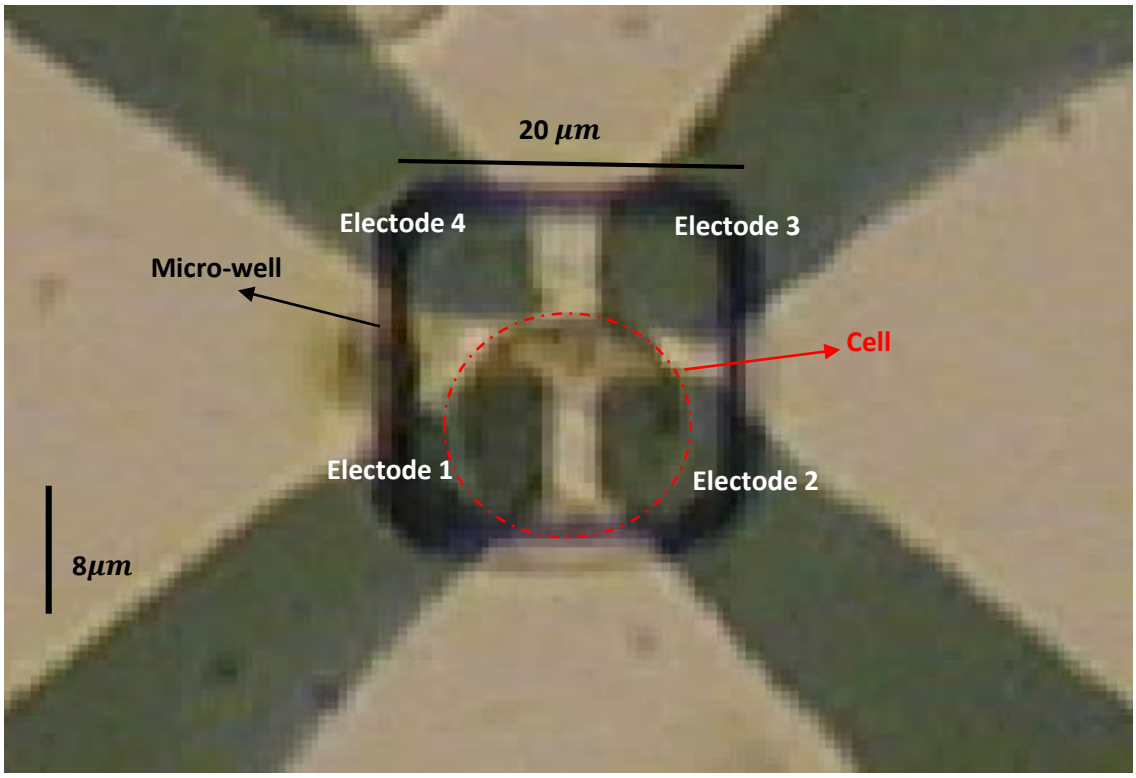

Figure 4-6. Trapped cell on top of the 4 electrodes.

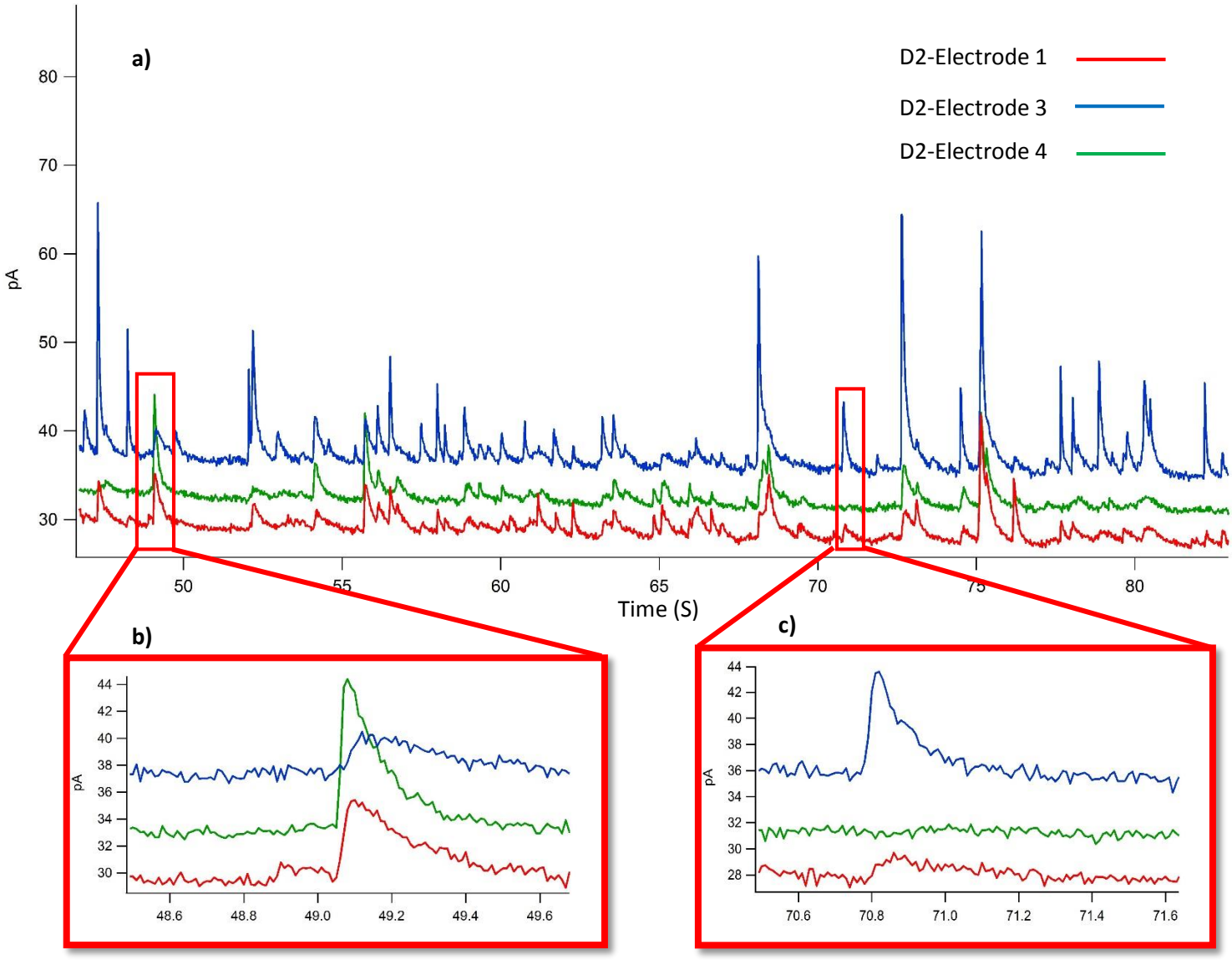

Figure 4-7. Amperometery recording of a single cell. a) Overlaying the recordings obtained from electrodes 13, 4, and 6 of Amplifier D2. b) Three electrodes are showing signal. c) Only two electrodes showed signal.

Recordings were made with a low-pass filter with a corner frequency of 500 Hz, a sampling rate of 1000 s^{-1}, and a final digital low-pass filter setting of 100 Hz. The electrode voltage was 600 mV relative to the Ag/AgCl reference electrode.

Figure 4-7 depicts sample amperometeric spikes obtained from channels 1, 3, and 4 of the amplifier D2. For those events that were detected in all three channels, it is possible to predict the location of the release with a very good precision as described in Section 4-4. However, for the events detected with only two electrodes, the release site can only be localized to a line between those two electrodes.

4-3. Analysis of spike parameters

The parameters from each spike were measured using analysis software(Segura, Brioso et al. 2000) and the results are shown in table 4-1. It can be seen that electrode 3 recorded 69 spikes whereas electrode 4 and 1 recorded 44 and 26 spikes, respectively. In order to determine whether electrodes are effectively oxidizing the molecules, each individual electrode should at least record one spike with a t_{peak} of <20 ms, otherwise the experiment would be discarded(Hafez, Kisler et al. 2005). Figure 4-9 shows the histogram of t_{peak} for electrodes 1, 3, and 4 . It can be seen that all electrode recorded at least one event with a t_{peak} <20 ms.

	26 events were recorded by electrode 1			
	t_peak (ms)	t_half	Peak current (pA)	Charge (pC)
Mean	45.36	90.39	7.78	1.08
SEM	4.78	6.59	0.92	0.14
	69 events were recorded by electrode 3			
	t_peak (mS)	t_half	Peak current (pA)	Charge (pC)
Mean	22.20	51.14	12.14	0.95
SEM	1.79	3.37	0.78	0.08
	44 events were recorded by electrode 4			
	t_peak(mS)	t_half	Peak current (pA)	Charge (pC)
Mean	39.37	76.86	6.00	0.78
SEM	3.34	5.45	0.55	0.09

Table 4-1. Mean and SEM values of t_peak, t1_half, peak Current, and recorded charge by each electrode.

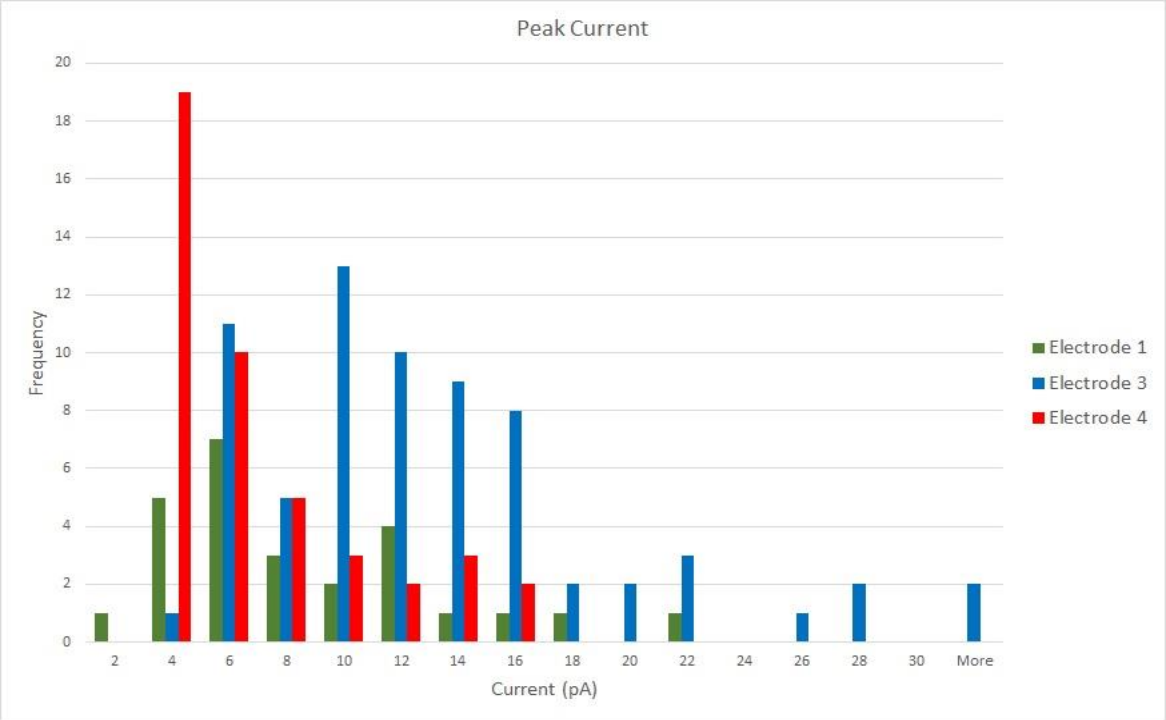

Figure 4-8. Peak Current histogram of Electrodes 1, 3, 4 from 23, 69, 44 events respectively.

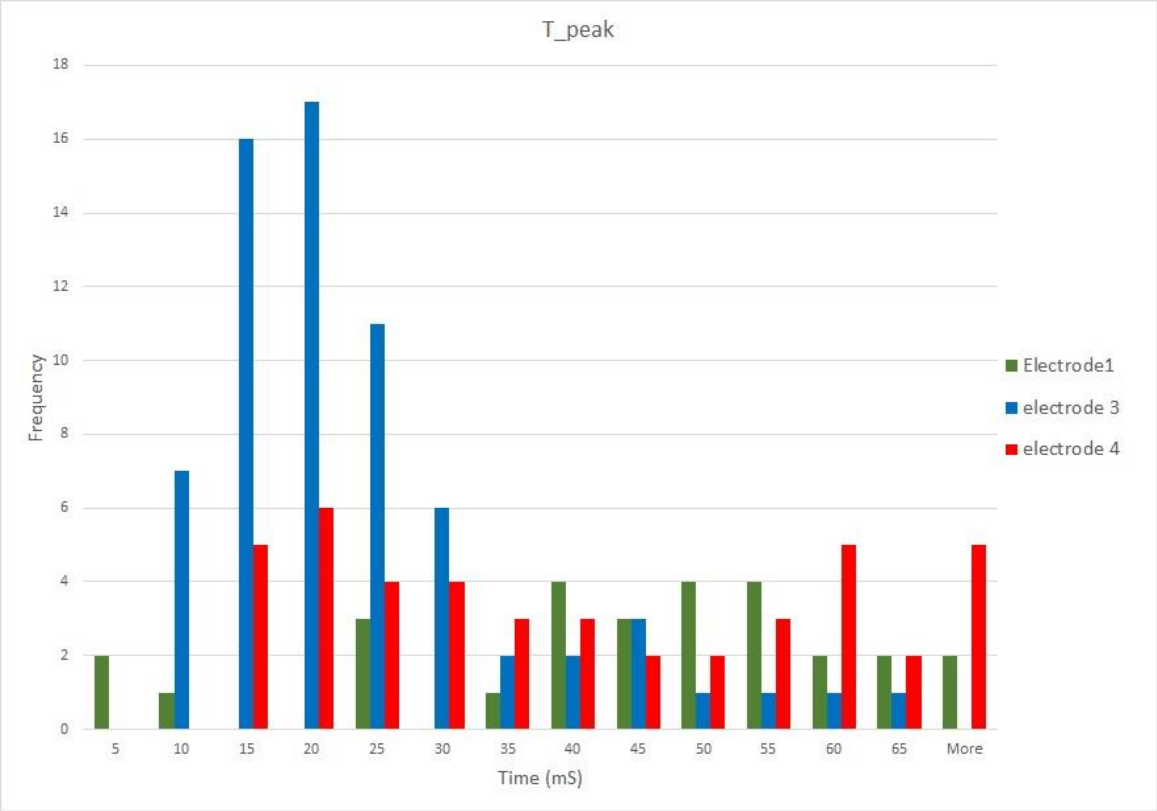

Figure 4-9. t_peak histogram of Electrodes 1, 3, 4 from 23,69, 44 events respectively.

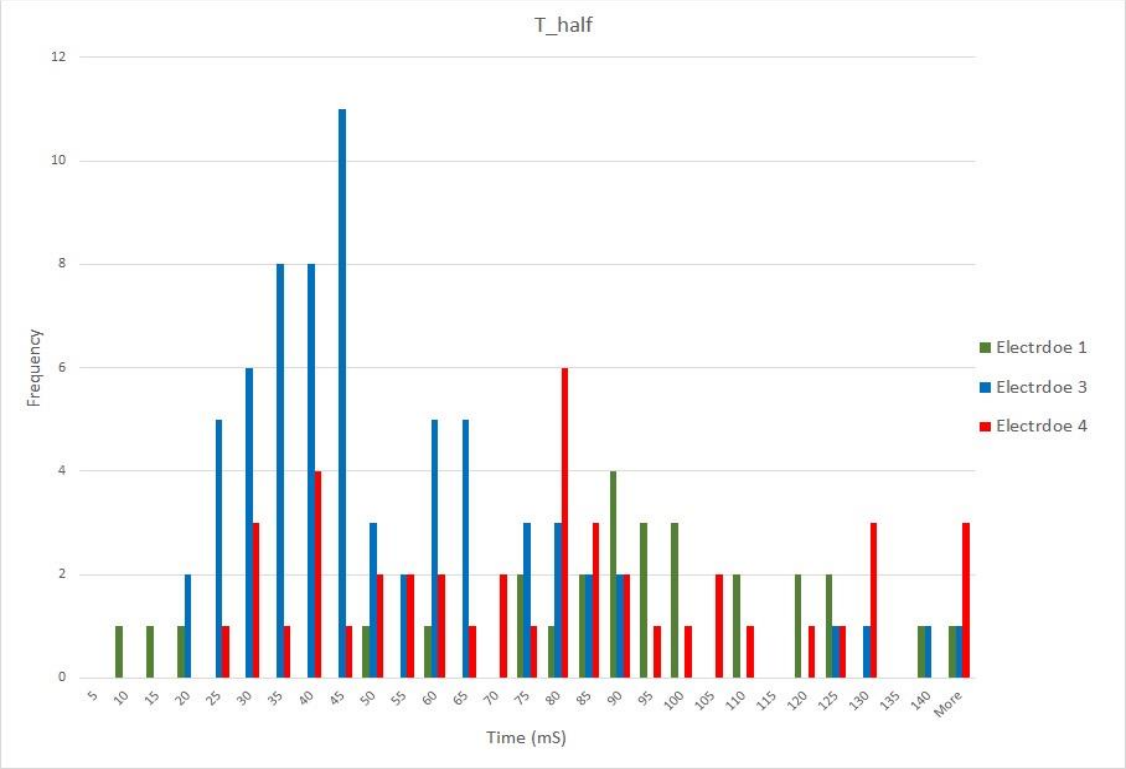

Figure 4-10. t_half histogram of Electrodes 1, 3, 4 from 23, 69, 44 events respectively.

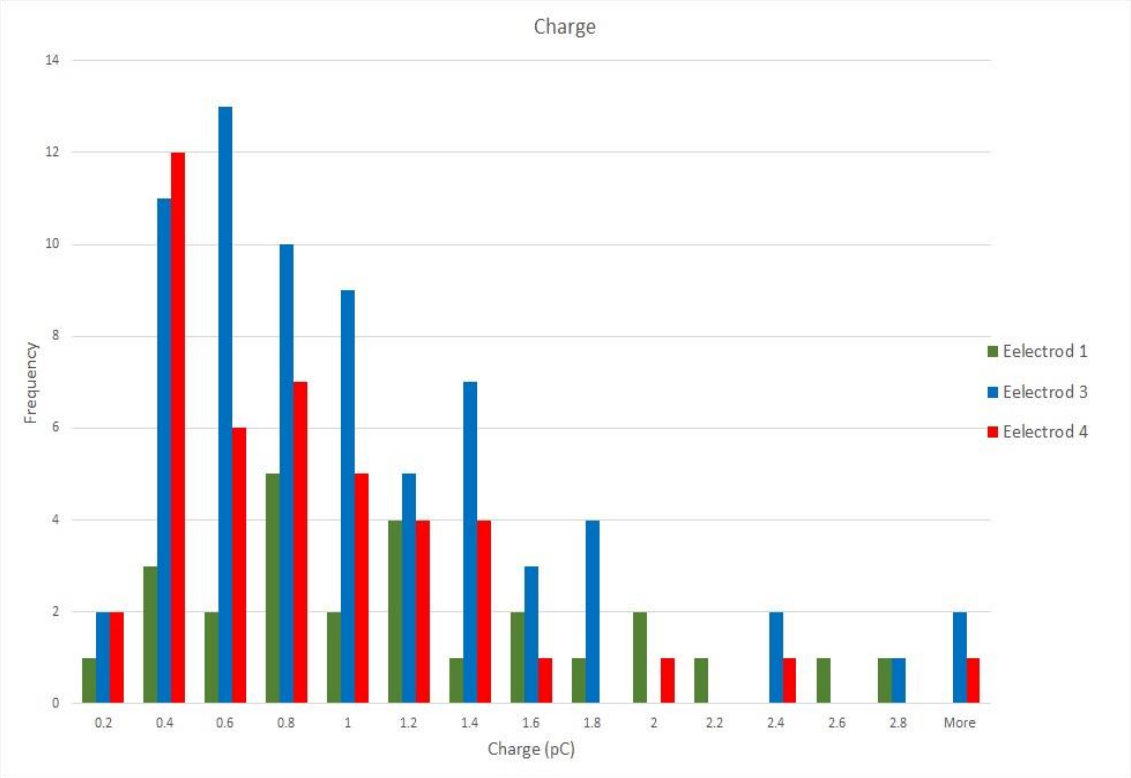

Figure 4-11. Charge histogram of Electrodes 1, 3, 4 from 23, 69, 44 events respectively.

It was mentioned earlier in the introduction chapter that half width time (t_half) reflects both the time for catecholamine to be released from the vesicle and the diffusion time to the electrode. From the table 4-1 it can be seen that the mean value of the t_half is longer for electrode 1 than for electrode 3, so perhaps more exocytosis events occur closer to electrode 3.

4-4. Electrochemical imaging of the release sites

Spikes detected in at least three electrodes were identified using custom MATLAB software. The total charge of each individual event was integrated and the fractional charge of each electrode in each event was considered as the charge detected by that electrode divided by the total charge of the event. To localize the event, the Least Square Mean (LSM) method was employed to obtain the best agreement between the simulated and experimental data. The point on the grid that had the least error was identified as the location of the release event(Hafez, Kisler et al. 2005). The COMSOL simulation was done on the cell with a grid resolution of 0.5 μm. Table 4-2 shows the location coordinate of the identified events that were detected in three electrodes.

Event	Time (s)	Partial charge detected by Electrode 1	Partial charge detected by Electrode 2	Partial charge detected by Electrode 3	Total Charge	X (μm)	Y (μm)
1	4.36	0.09	0.47	0.44	7.10	0	2
2	13.69	0.02	0.75	0.23	1.67	2	2.5
3	31.32	0.22	0.47	0.31	5.53	0.5	1
4	49.08	0.05	0.7	0.25	3.56	1.5	2.5
5	75.14	0.06	0.42	0.52	6.00	-0.5	2.5
6	83.90	0.12	0.62	0.26	3.17	1	1.5
7	116.51	0.04	0.50	0.46	3.40	0	2.5
8	119.02	0.02	0.51	0.47	1.38	0	2.5
9	119.76	0.04	0.57	0.39	1.78	0.5	2.5
10	125.36	0.05	0.62	0.33	1.98	1	2.5
11	135.38	0.07	0.58	0.35	3.90	0.5	2.5

Table 4-2. Partial detected charge by each electrode. The release sites were assigned based on the best agreement, obtained from Mean Least Square (MLS) error, between the experimental results and the results from the simulation.

The mean value of the total charge was 3.59$\pm$0.58 pC, which is close to what is reported by the Lindau lab(Hafez, Kisler et al. 2005). Note that this value is significantly larger than the mean charge of all spikes detected, presumably because the requirement that a spike is detected in more than two electrodes means that only large release events can be localized. As can be seen in Table 4-2, the detected events are mostly in the proximity of the point (X=0.5, Y=2.5 μm) where, X=0 and Y=0 is the center of the micro-well. Recall that only release from the part of the cell that is closer to the middle of the microwell is likely to be detected by three electrodes and thus be localized. In this experiment, the cell was not located in the center of the microwell, and the location of the detected events is indicated in Fig. 4-8. Note that events are not detected if they occur too close to one of the electrodes since most of the molecules get oxidized by the nearby electrode and other electrodes cannot

record a detectable signal. Also note that no events are detected near electrode number 2 since this was non-functional.

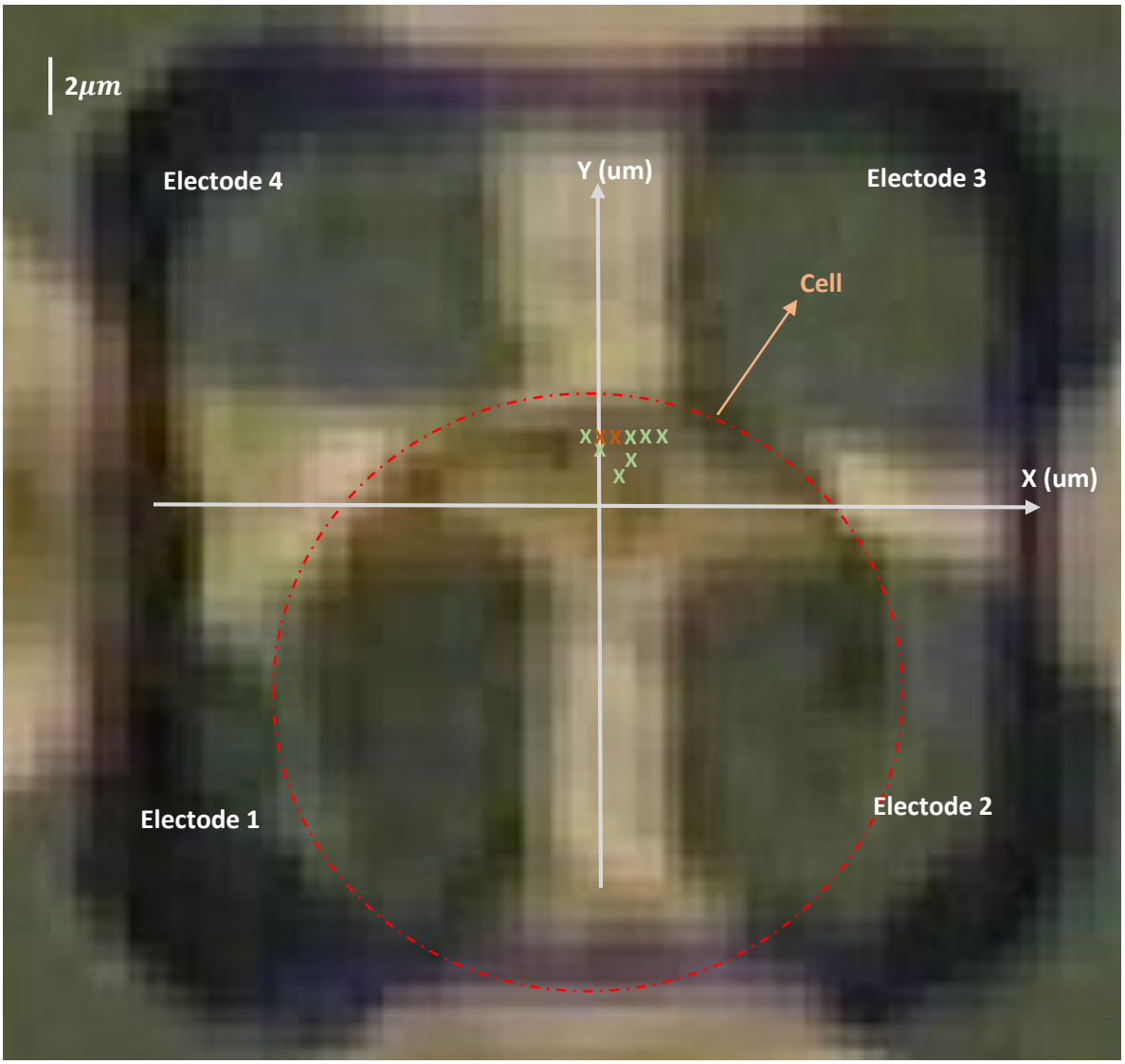

Figure 4-12. Release events were detected in the proximity of the point X=0, Y=2.5 μm. The dashed red circle shows the position of the cell. Green crosses depict the spots that exocytosis events were detected. The green 'X's are points that only one event was identified whereas two events were identified on the red 'X's.

The location of the cell in microwell is very important and can affect the electrochemical imaging. Figure 4-8 shows that the microwell is probably too big for chromaffin cells and as a result of that the cell could not be targeted at the center of the microwell. If the cell is too small, it might not extend into the central area of the microwell and we could never detect any of the events. This problem can be addressed by redesigning the SU8 mask layout in order to make smaller microwells.

Chapter V. Future Direction and Conclusion

5-1. Introduction

A limitation of the four-electrode method is that only release events occurring in the central area of the four electrodes can be localized. For localizing an event, it is essential that we get an acceptable signal to noise ratio from at least three electrodes. For the events which are happening too close to one or two of the electrodes, the closer electrodes oxidize the majority of molecules released while very few molecules remains to reach the other electrode surfaces. One possible way to tackle this problem is to make the size of electrodes smaller so that the distance between the cell and electrodes will be increased. In this case however, molecules have to travel a longer distance to reach to the surface of electrodes and the width of the amperometric spike will increase whereas the peak of observed signal will decrease, resulting in a poor signal-to-noise ratio. Therefore, there is a tradeoff between having smaller or larger electrodes. The main purpose of this chapter is to suggest a simulation-guided approach to optimize the size and the geometry of the electrodes in order to increase the area in which the exocytosis events can be detected through the electrochemical imaging technique.

5-2. Simulation-guided improvements of electrochemical electrode arrays for electrochemical imaging

Here I propose a design with curved electrodes and perform COMSOL simulations to see if it can expand the area in which exocytosis events can be detected (figure 5-1).

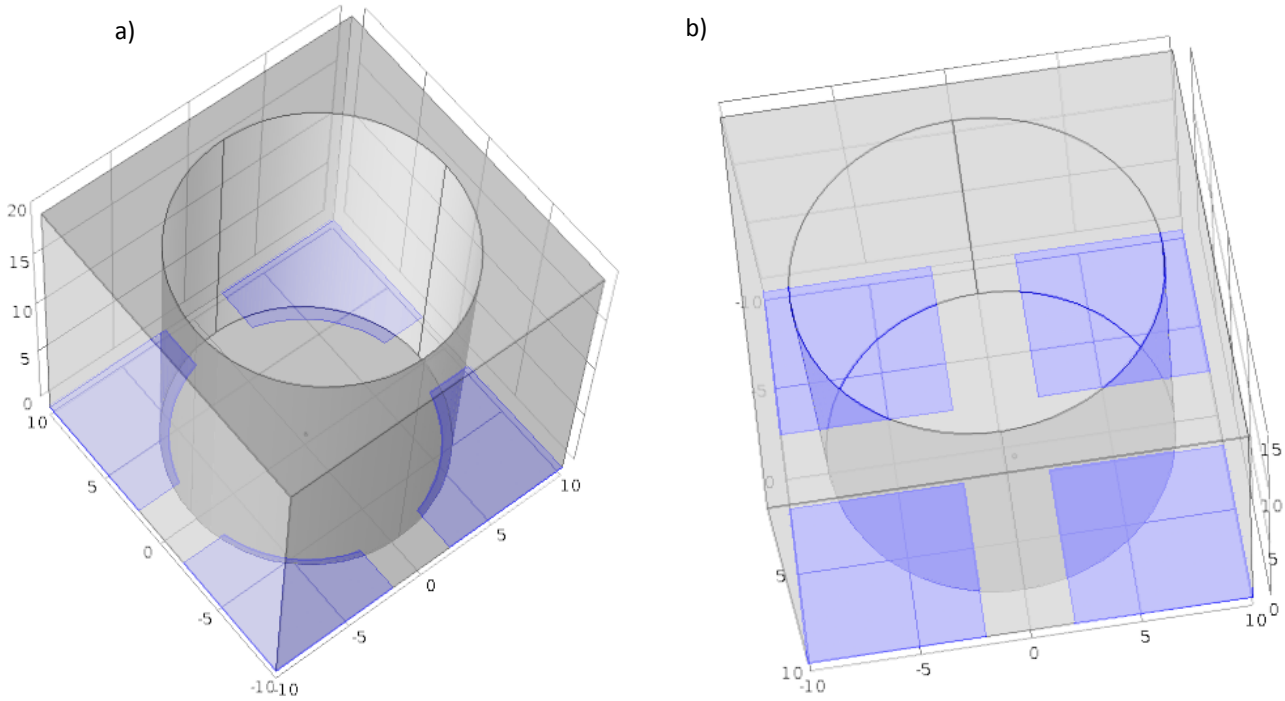

Figure 5-1. a) The improved design with circular electrodes. b) The previous design with square electrodes.

For this simulation, only those events are considered detectable if they fulfill these two conditions:

1) The peak current in at least three of the electrodes must be >1 pA so that the signal can be distinguished from noise. 2) At least three electrodes must record >5% of the total recorded charge by all of the electrodes or else localization is imprecise.

I developed MATLAB software to extract the features (peak current and partial charge) from simulations. Figure 4-2 depicts the release sites in the test grid that meet the two conditions. In the new design, the area on the cell in which the exocytosis events can be detected is expanded by approximately 45 percent compared to the previous design. In the previous design 111 out of 363 grid points were marked as

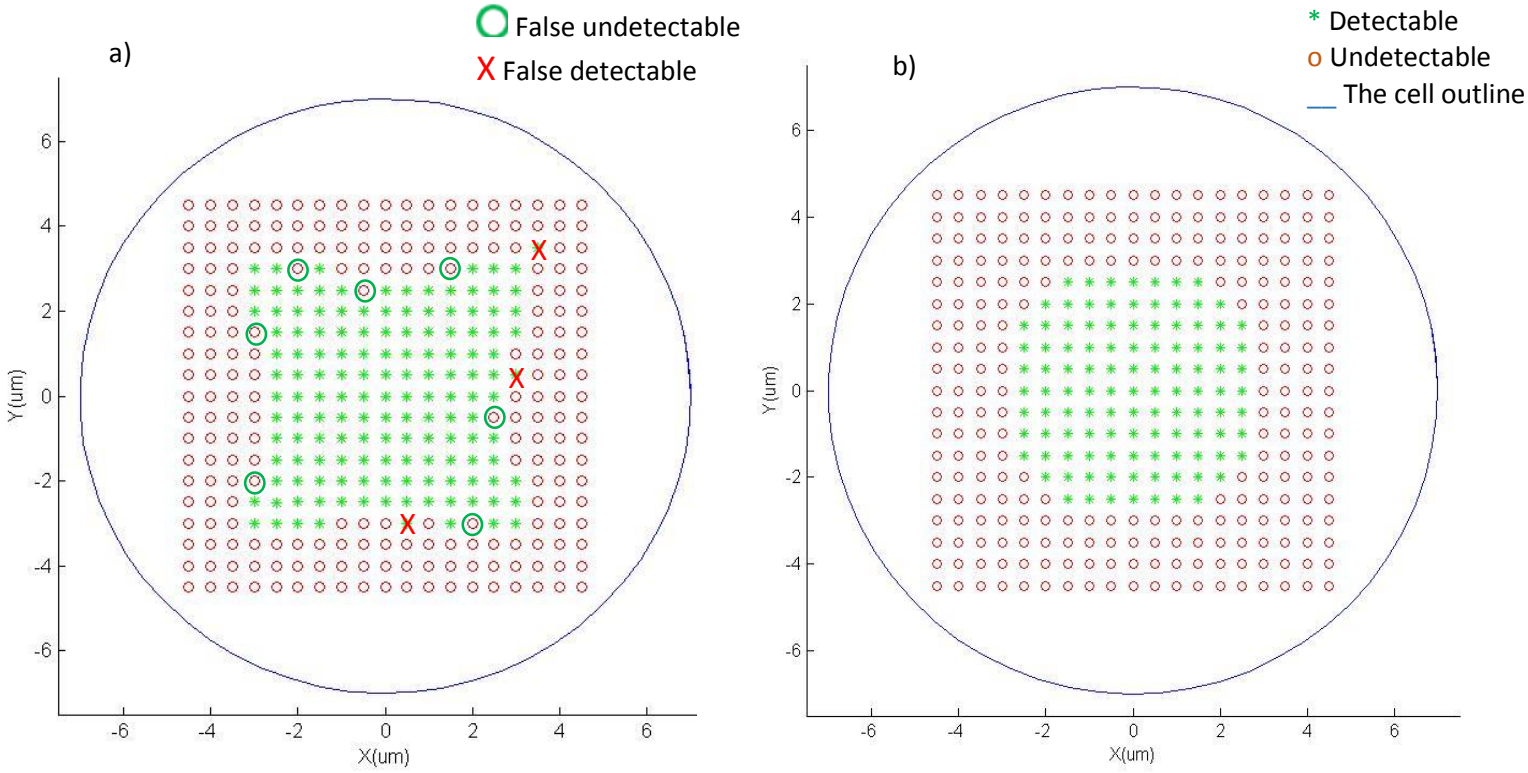

Figure 5-2. The detectable grids are shown with the green asterisks (*) vs. the undetectable grids which are depicted with the red circles (o) on the cells. a) The improved design with circular electrodes. b) The previously used design with square electrodes. The False undetectable and detectable spots are shown by ○ , X respectivly.

detected whereas in the curved-electrode design 161 out of 363 grid points were detected.

Even with the finest and best meshing algorithm FEM gives an approximate solution due to which the border between the detectable and undetectable area can be noisy and as a result the identify false detectable/ undetectable spots. Since the design of the simulation is symmetric, it is expected that the detectable/ undetectable spots are symmetric as well. Based on this assumption, false detectable/ undetectable spots are marked in figure 5-2.

5-3. Conclusion

In order to perform electrochemical imaging, four square microelectrodes located in a 20 um square microwell were fabricated through photolithographic techniques. A high density of chromaffin cells were placed in the solution reservoir on top of the electrode arrays, and individual cells settled into microwells. Upon cell stimulation with a high potassium concentration, amperometric recordings of exocytois were performed successfully. The data obtained from cell recordings were compared with the simulation data obtained from FEM modeling and the locations of release sites were identified.

Due to the practical requirement that a significant fraction of released molecules must be detected by at least three electrodes, electrochemical imaging can only be successfully applied in the central area between the four electrodes. This is the main limitation of this method since we must discard many of events that occur in the areas farther from the center. In order to address this issue, a simulation-guided electrode re-design was tested using FEM simulations. The simulation showed that the improved design is predicted to increase the area of detection by approximately 45% compared to the design used in cell tests.

Appendix

RWS code through IGOR PRO

```
#pragma rtGlobals=1      // Use modern global access method
and strict wave access.
function four_Sqr_elec_3D (npart,niter,l,el,x0,y0,z0)
Variable npart  // number of particles
Variable niter   // number of iteration (usec)
Variable l // dimensions in um
Variable el // size of electrode
Variable x0,y0,z0   //initial position in x,y of the event
Variable D = 8e-5   // diffusion coef of catecholamine under
cell, um^2/us
Variable std = sqrt(2*D)  // std dev of step in 1 us
Variable xval, yval, zval
Variable genx,geny,genz
Make /n=1/ o esc =0

Make /n=(npart) /o eq1,eq2,eq3,eq4,knum, xf,yf,zf

Variable i,j

for ( j=1; j<=npart; j+=1)
      i=0
     xval = x0
     yval = y0
     zval=  z0
     genz=0

     do
          genx = gnoise(std)
          geny = gnoise(std)
          xval += genx
          yval += geny
          if ((xval^2 +yval^2)> 64)
          genz=gnoise(std)
          zval += genz
          endif
          i+=1
```

```
          // reflecting bouandry condition of the walls
          if ((xval<-l || xval>l || yval<-l || yval>l ||
zval<0) && zval<= 16)
          xval-=genx
          yval-=geny
          zval-=zval
          i-=1
          knum[j]+=1
          endif
          // reflecting bouandry condition of the cell walls
"cell diameter is considered as semifinite cylender with 16
um of diameter"
          if (zval>0 && zval<=16 && (xval^2+yval^2)<64)
          xval-=genx
          yval-=geny
          zval-=zval
          i-=1
          knum[j]+=1
          endif

          // escaping particles
          if (zval>16 || xval >l+1 || xval<-l-1 || yval>l+1
|| yval<-l-1)
          i=niter
          esc+=1
          endif
     while((i<niter) && (xval>-l+el || yval>-l+el || zval>
0.04)&& (xval<l-el || yval>-l+el || zval> 0.04) && (xval<l-el
|| yval<l-el || zval> 0.04) && (xval>-l+el || yval<l-el ||
zval> 0.04))
     if (xval<=-l+el && yval<=-l+el && zval<= 0.04)
     eq1[ j]=i
     elseif (xval>=l-el && yval<=-l+el && zval<= 0.04)
     eq2[ j]=i
     elseif (xval>=l-el && yval>=l-el && zval<= 0.04)
     eq3[ j]=i
     elseif (xval<=-l+el && yval>=l-el && zval<= 0.04)
     eq4[ j]=i
     endif
xf[j]=xval
yf[j]=yval
```

```
zf[j]=zval
endfor

wave eq1
eq1 = eq1[p] == 0 ? NaN : eq1[p]
eq2 = eq2[p] == 0 ? NaN : eq2[p]
eq3 = eq3[p] == 0 ? NaN : eq3[p]
eq4 = eq4[p] == 0 ? NaN : eq4[p]
WaveTransform zapNaNs, eq1
WaveTransform zapNaNs, eq2
WaveTransform zapNaNs, eq3
WaveTransform zapNaNs, eq4
WaveTransform zapNaNs, eq4
// to make the time axis based on second (S)
eq1 /= 1e6
eq2 /= 1e6
eq3 /= 1e6
eq4 /= 1e6
Make/N=82/O eq1_Hist, eq2_Hist, eq3_Hist, eq4_Hist
Histogram/B=1 eq1,eq1_Hist
Histogram/B=1 eq2,eq2_Hist
Histogram/B=1 eq3,eq3_Hist
Histogram/B=1 eq4,eq4_Hist
duplicate /o eq1_Hist, normal1
duplicate /o eq2_Hist, normal2
duplicate /o eq3_Hist, normal3
duplicate /o eq4_Hist, normal4
variable maxi_elec1, maxi_elec2, maxi_elec3, maxi_elec4 //
maximum of wave
maxi_elec1= wavemax(normal1)
maxi_elec2= wavemax(normal2)
maxi_elec3= wavemax(normal3)
maxi_elec4= wavemax(normal4)

normal1/=maxi_elec1
normal2/=maxi_elec2
normal3/=maxi_elec3
normal4/=maxi_elec4
// the Histograms in terms of current (pA) is
duplicate /o eq1_Hist, i_e1
duplicate /o eq2_Hist, i_e2
```

```
duplicate /o eq3_Hist, i_e3
duplicate /o eq4_Hist, i_e4
 i_e1=((3.12e6/npart)*(2*1.602e-19)*eq1_Hist)*1e12/(5e-3)
 i_e2=((3.12e6/npart)*(2*1.602e-19)*eq2_Hist)*1e12/(5e-3)
 i_e3=((3.12e6/npart)*(2*1.602e-19)*eq3_Hist)*1e12/(5e-3)
 i_e4=((3.12e6/npart)*(2*1.602e-19)*eq4_Hist)*1e12/(5e-3)
 //displaying the RWS current
 Display i_e1,i_e2,i_e3,i_e4
 Label bottom "Time (S)"
 Label left "Current (pA)"
end
```

Finding simultaneous amperometric recording by different electrodes through MATLAB

```
close all
clear all
clc
%% Importing data
elec4=xlsread('elec4.xlsx');
elec6=xlsread('elec6.xlsx');
elec13=xlsread('elec13.xlsx');

%% identifying same events

%the number of the recoreded event by each electrode
 len_e4= length(elec4);
 len_e6= length(elec6);
 len_e13= length(elec13);

 %the simultanious event
 event46=zeros(len_e4,1);
 row_num4=zeros(len_e4,1);
 row_num6=zeros(len_e4,1);
 row_num13=zeros(len_e4,1);
 event4613=zeros(len_e4,1);
 row_num4613=zeros(len_e4,1);

for k=1:len_e13
    for i=1:len_e4
        if abs(elec4(i,3)-elec13(k,3))<0.5
```

```
            for j=1:len_e6
                if abs(elec4(i)-elec6(j,3))<0.9
                   event4613(i)=elec4(i);
                   row_num4(i,1)=i;
                   row_num6(i,1)=j;
                   row_num13(i,1)=k;
                end
            end
        end
    end
end
event4613(event4613==0)=[];
event4613;
row_num4(row_num4==0)=[];
row_num6(row_num6==0)=[];
row_num13(row_num13==0)=[];
row_num4;
row_num6;
row_num13;
[elec4(row_num4) elec6(row_num6) elec13(row_num13)]
charge1=[elec4(row_num4,6) elec6(row_num6,6)
elec13(row_num13,6)];
total_event_charge=sum(charge1,2);
partial_charge=charge1./(total_event_charge*ones(1,size(charg
e1,2)));
partial_charge=[elec4(row_num4,3) partial charge];
```

Feature extraction from simulation results through MATLAB

```
close all
clear all
clc
%adding noise to actual data
data_set1=xlsread('110215.xlsx');

%len1  is the length of the modified  data
len1=length(data_set1);
%%
%%Initialzing the data
```

```
t_res=data_set1(2,3)-data_set1(1,3);
%i is the no of data set for each each grid
len0=2;
while data_set1(len0,3)~= 0
      len0=len0+1;
end
%len0 is the length of each grid
len0=len0-1;
nu_grids=len1/len0;
charge_e=zeros(nu_grids,4);
total_charge=zeros(nu_grids,1);
partial_charge=zeros(nu_grids,4);

%modifying data

for z=1:len0:len1
    data_set1(z:z+4,4:end)=0;
end

%% Feature extraction
 grid=1;
for z=1:len0:len1
    for elec=1:4
        charge_e(grid,elec)=trapz(data_set1(z:z+len0-
1,3),data_set1(z:z+len0-1,elec+3));
    end
    grid=grid+1;
end

grids=data_set1(1:len0:len1,1:2).*1e6;
charge_e(:,1)=[];
total_charge=sum(charge_e,2);
frac_charge=charge_e./(total_charge*ones(1,3));
features=[grids, frac_charge];
```

Finding the best fit between the simulation and the experimental data

```
%Mean Square Root
clear
clc
sim_data=xlsread('par_char_sim_new');
real_data=xlsread('par_char_exp');
real_len=length(real_data);
sim_len=length(sim_data);
sqe_root=zeros(sim_len,1);
grids=zeros(real_len,6);

for i=1:real_len
    for j=1:sim_len
        %sqt=sqrt(sum((real_data(i,2:end)-
sim_data(j,3:end)).^2,2));
        sqe_root(j)= sqrt(sum((real_data(i,2:end)-
sim_data(j,3:end)).^2,2))/3;
    end
    min_sqr=min(sqe_root);
    [row, col]=find(sqe_root==min_sqr);
    grids(i,:)= [real_data(i,:) sim_data(row,1:2)];
end
grids
```

References

Abel, P. and T. von Woedtke (2002). "Biosensors for in vivo glucose measurement: can we cross the experimental stage." Biosensors and Bioelectronics **17**(11): 1059-1070.

Albillos, A., et al. (1997). "The exocytotic event in chromaffin cells revealed by patch amperometry." Nature **389**(6650): 509-512.

Alés, E., et al. (1999). "High calcium concentrations shift the mode of exocytosis to the kiss-and-run mechanism." Nature Cell Biology **1**(1): 40-44.

Anderson, D. R. (2001). "The need to get the basics right in wildlife field studies." Wildlife Society Bulletin: 1294-1297.

Ashery, U., et al. (1999). "An efficient method for infection of adrenal chromaffin cells using the Semliki Forest virus gene express1on system." European journal of cell biology **78**(8): 525-532.

Bogue, R. (2013). "Recent developments in MEMS sensors: a review of applications, markets and technologies." Sensor Review **33**(4): 300-304.

Breckenridge, L. J. and W. Almers (1987). "Currents through the fusion pore that forms during exocytosis of a secretory vesicle." Nature **328**(6133): 814-817.

Burgoyne, R. D. and A. Morgan (2003). "Secretory granule exocytosis." Physiological reviews **83**(2): 581-632.

Butz, S., et al. (1998). "A tripartite protein complex with the potential to couple synaptic vesicle exocytosis to cell adhesion in brain." Cell **94**(6): 773-782.

Chang, T. Y., et al. (2007). "Cell and protein compatibility of parylene-C surfaces." Langmuir **23**(23): 11718-11725.

Chow, R. H., et al. (1992). "Delay in vesicle fusion revealed by electrochemical monitoring of single secretory events in adrenal chromaffin cells." Nature **356**(6364): 60-63.

Chow, R. H., et al. (1992). "Delay in vesicle fusion revealed by electrochemical monitoring of single secretory events in adrenal chromaffin cells."

De Toledo, G. A., et al. (1993). "Release of secretory products during transient vesicle fusion." Nature **363**(6429): 554-558.

Dias, A. F., et al. (2002). "An electrochemical detector array to study cell biology on the nanoscale." Nanotechnology **13**(3): 285.

Edwardson, J. M., et al. (2003). "Expression of Mutant Huntingtin Blocks Exocytosis in PC12 Cells by Depletion of Complexin II." Journal of Biological Chemistry **278**(33): 30849-30853.

Evanko, D. (2005). "Primer: spying on exocytosis with amperometry." Nature methods **2**(9): 650-650.

Fenwick, E., et al. (1978). "Functional and morphological characterization of isolated bovine adrenal medullary cells." The Journal of cell biology **76**(1): 12-30.

Gao, Y., et al. (2009). "A microfluidic cell trap device for automated measurement of quantal catecholamine release from cells." Lab on a Chip **9**(23): 3442-3446.

Gao, Y., et al. (2008). "Magnetron sputtered diamond-like carbon microelectrodes for on-chip measurement of quantal catecholamine release from cells." Biomedical microdevices **10**(5): 623-629.

Gillis, K., et al. (1991). "Single cell assay of exocytosis from adrenal chromaffin cells using “perforated patch recording”." Pflügers Archiv **418**(6): 611-613.

Gillis, K. D. and R. H. Chow (1997). "Kinetics of exocytosis in adrenal chromaffin cells." Seminars in Cell & Developmental Biology **8**(2): 133-140.

Glavinović, M., et al. (1998). "Comparison of vesicular volume and quantal size in bovine chromaffin cells." Neuroscience **85**(3): 957-968.

Grayson, A. C. R., et al. (2004). "A BioMEMS review: MEMS technology for physiologically integrated devices." Proceedings of the IEEE **92**(1): 6-21.

Hafez, I., et al. (2005). "Electrochemical imaging of fusion pore openings by electrochemical detector arrays." Proceedings of the National Academy of Sciences of the United States of America **102**(39): 13879-13884.

Hamill, O. P., et al. (1981). "Improved patch-clamp techniques for high-resolution current recording from cells and cell-free membrane patches." Pflügers Archiv **391**(2): 85-100.

Heiskanen, A., et al. (2008). Development of a microfluidic on-line culture system for combined electrochemical and optical real-time detection of cellular processes. Proceeding of the Twelfth International Conference on Miniaturized Systems for Chemistry and Life Sciences.

Ho, C.-M. and Y.-C. Tai (1996). "REVIEW: MEMS and Its Applications for Flow Control." Journal of Fluids Engineering **118**(3): 437-447.

Jahn, R. and R. H. Scheller (2006). "SNAREs—engines for membrane fusion." Nature reviews Molecular cell biology **7**(9): 631-643.

Kisler, K., et al. (2012). "Transparent electrode materials for simultaneous amperometric detection of exocytosis and fluorescence microscopy." J Biomater Nanobiotechnol **3**(2A): 243.

Klyachko, V. A. and M. B. Jackson (2002). "Capacitance steps and fusion pores of small and large-dense-core vesicles in nerve terminals." Nature **418**(6893): 89-92.

Knight, D. E., et al. (1985). "Inhibition of exocytosis in bovine adrenal medullary cells by botulinum toxin type D." Nature **317**(6039): 719-721.

Kotzar, G., et al. (2002). "Evaluation of MEMS materials of construction for implantable medical devices." Biomaterials **23**(13): 2737-2750.

Lin, R. C. and R. H. Scheller (2000). "Mechanisms of synaptic vesicle exocytosis." Annual review of cell and developmental biology **16**(1): 19-49.

Lindau, M. and G. Alvarez de Toledo (2003). "The fusion pore." Biochimica et Biophysica Acta (BBA) - Molecular Cell Research **1641**(2–3): 167-173.

Liu, X., et al. (2011). "Microwell device for targeting single cells to electrochemical microelectrodes for high-throughput amperometric detection of quantal exocytosis." Analytical chemistry **83**(7): 2445-2451.

Meng, E. and Y.-C. Tai (2005). Parylene etching techniques for microfluidics and bioMEMS. Micro Electro Mechanical Systems, 2005. MEMS 2005. 18th IEEE International Conference on, IEEE.

Neher, E. and A. Marty (1982). "Discrete changes of cell membrane capacitance observed under conditions of enhanced secretion in bovine adrenal chromaffin cells." Proceedings of the National Academy of Sciences **79**(21): 6712-6716.

Nemani, K. V., et al. (2013). "In vitro and in vivo evaluation of SU-8 biocompatibility." Materials Science and Engineering: C **33**(7): 4453-4459.

Nguyen, N.-T. and Z. Wu (2005). "Micromixers—a review." Journal of Micromechanics and Microengineering **15**(2): R1.

R. Colin Johnson, A. T. E., EE Times.

Santini, J. T., et al. (2000). "Microchip technology in drug delivery." Annals of medicine **32**(6): 377-379.

Schneider, S. (2001). "Kiss and run mechanism in exocytosis." Journal of Membrane Biology **181**(2): 67-76.

Segura, F., et al. (2000). "Automatic analysis for amperometrical recordings of exocytosis." Journal of neuroscience methods **103**(2): 151-156.

Smith, P. A., et al. (1999). "Quantal analysis of 5-hydroxytryptamine release from mouse pancreatic β-cells." The Journal of Physiology **521**(3): 651-664.

Südhof, T. C. (1995). "The synaptic vesicle cycle: a cascade of protein protein interactions."

Sun, X. and K. D. Gillis (2006). "On-chip amperometric measurement of quantal catecholamine release using transparent indium tin oxide electrodes." Analytical chemistry **78**(8): 2521-2525.

Sutton, R. B., et al. (1998). "Crystal structure of a SNARE complex involved in synaptic exocytosis at 2.4[thinsp]A resolution." Nature **395**(6700): 347-353.

Tanaka, M. (2007). "An industrial and applied review of new MEMS devices features." Microelectronic Engineering **84**(5–8): 1341-1344.

Trouillon, R., et al. (2013). "Evaluating the Diffusion Coefficient of Dopamine at the Cell Surface During Amperometric Detection: Disk vs Ring Microelectrodes." Analytical Chemistry **85**(13): 6421-6428.

Vernekar, V. N., et al. (2009). "SU-8 2000 rendered cytocompatible for neuronal bioMEMS applications." Journal of Biomedical Materials Research Part A **89**(1): 138-151.

Voets, T., et al. (2001). "Munc18-1 promotes large dense-core vesicle docking." Neuron **31**(4): 581-592.

Wightman, R. M., et al. (1991). "Temporally resolved catecholamine spikes correspond to single vesicle release from individual chromaffin cells." Proceedings of the National Academy of Sciences of the United States of America **88**(23): 10754-10758.

Yang, Y., et al. (2007). "Phosphomimetic mutation of Ser-187 of SNAP-25 increases both syntaxin binding and highly Ca2+-sensitive exocytosis." The Journal of general physiology **129**(3): 233-244.

Yao, J. and K. D. Gillis (2012). "Quantification of noise sources for amperometric measurement of quantal exocytosis using microelectrodes." Analyst **137**(11): 2674-2681.